ISSN: 2395-6992

Engineering Journal: IJOER

Volume-10, Issue-10,
October 2024

www.ijoer.com

DOWNLOAD

Preface

We would like to present, with great pleasure, the inaugural volume-10, Issue-10, October 2024, of a scholarly journal, *International Journal of Engineering Research & Science*. This journal is part of the AD Publications series *in the field of Engineering, Mathematics, Physics, Chemistry and science Research Development*, and is devoted to the gamut of Engineering and Science issues, from theoretical aspects to application-dependent studies and the validation of emerging technologies.

This journal was envisioned and founded to represent the growing needs of Engineering and Science as an emerging and increasingly vital field, now widely recognized as an integral part of scientific and technical investigations. Its mission is to become a voice of the Engineering and Science community, addressing researchers and practitioners in below areas:

Chemical Engineering	
Biomolecular Engineering	Materials Engineering
Molecular Engineering	Process Engineering
Corrosion Engineering	
Civil Engineering	
Environmental Engineering	Geotechnical Engineering
Structural Engineering	Mining Engineering
Transport Engineering	Water resources Engineering
Electrical Engineering	
Power System Engineering	Optical Engineering
Mechanical Engineering	
Acoustical Engineering	Manufacturing Engineering
Optomechanical Engineering	Thermal Engineering
Power plant Engineering	Energy Engineering
Sports Engineering	Vehicle Engineering
Software Engineering	
Computer-aided Engineering	Cryptographic Engineering
Teletraffic Engineering	Web Engineering
System Engineering	
Mathematics	
Arithmetic	Algebra
Number theory	Field theory and polynomials
Analysis	Combinatorics
Geometry and topology	Topology
Probability and Statistics	Computational Science
Physical Science	Operational Research
Physics	
Nuclear and particle physics	Atomic, molecular, and optical physics
Condensed matter physics	Astrophysics
Applied Physics	Modern physics
Philosophy	Core theories

Chemistry	
Analytical chemistry	Biochemistry
Inorganic chemistry	Materials chemistry
Neurochemistry	Nuclear chemistry
Organic chemistry	Physical chemistry
Other Engineering Areas	
Aerospace Engineering	Agricultural Engineering
Applied Engineering	Biomedical Engineering
Biological Engineering	Building services Engineering
Energy Engineering	Railway Engineering
Industrial Engineering	Mechatronics Engineering
Management Engineering	Military Engineering
Petroleum Engineering	Nuclear Engineering
Textile Engineering	Nano Engineering
Algorithm and Computational Complexity	Artificial Intelligence
Electronics & Communication Engineering	Image Processing
Information Retrieval	Low Power VLSI Design
Neural Networks	Plastic Engineering

Each article in this issue provides an example of a concrete industrial application or a case study of the presented methodology to amplify the impact of the contribution. We are very thankful to everybody within that community who supported the idea of creating a new Research with IJOER. We are certain that this issue will be followed by many others, reporting new developments in the Engineering and Science field. This issue would not have been possible without the great support of the Reviewer, Editorial Board members and also with our Advisory Board Members, and we would like to express our sincere thanks to all of them. We would also like to express our gratitude to the editorial staff of AD Publications, who supported us at every stage of the project. It is our hope that this fine collection of articles will be a valuable resource for *IJOER* readers and will stimulate further research into the vibrant area of Engineering and Science Research.

Mukesh Arora

(Chief Editor)

Board Members

Dr. M. Varatha Vijayan

Annauniversity Rank Holder, Commissioned Officer Indian Navy, Ncc Navy Officer (Ex-Serviceman Navy), Best Researcher Awardee, Best Publication Awardee, Tamilnadu Best Innovation & Social Service Awardee From Lions Club.

Dr. Mohamed Abdel Fatah Ashabrawy Moustafa

PhD. in Computer Science - Faculty of Science - Suez Canal University University, 2010, Egypt.

Assistant Professor Computer Science, Prince Sattam bin AbdulAziz University ALkharj, KSA.

Prof.S.Balamurugan

Dr S. Balamurugan is the Head of Research and Development, Quants IS & CS, India. He has authored/co-authored 35 books, 200+ publications in various international journals and conferences and 6 patents to his credit. He was awarded with Three Post-Doctoral Degrees - Doctor of Science (D.Sc.) degree and Two Doctor of Letters (D.Litt) degrees for his significant contribution to research and development in Engineering.

Dr. Mahdi Hosseini

Dr. Mahdi did his Pre-University (12^{th}) in Mathematical Science. Later he received his Bachelor of Engineering with Distinction in Civil Engineering and later he Received both M.Tech. and Ph.D. Degree in Structural Engineering with Grade "A" First Class with Distinction.

Dr. Anil Lamba

Practice Head – Cyber Security, EXL Services Inc., New Jersey USA.

Dr. Anil Lamba is a researcher, an innovator, and an influencer with proven success in spearheading Strategic Information Security Initiatives and Large-scale IT Infrastructure projects across industry verticals. He has helped bring about a profound shift in cybersecurity defense. Throughout his career, he has parlayed his extensive background in security and a deep knowledge to help organizations build and implement strategic cybersecurity solutions. His published researches and conference papers has led to many thought provoking examples for augmenting better security.

Dr. Ali İhsan KAYA

Currently working as Associate Professor in Mehmet Akif Ersoy University, Turkey.

Research Area: Civil Engineering - Building Material - Insulation Materials Applications, Chemistry - Physical Chemistry – Composites.

Dr. Parsa Heydarpour

Ph.D. in Structural Engineering from George Washington University (Jan 2018), GPA=4.00.

Dr. Heba Mahmoud Mohamed Afify

Ph.D degree of philosophy in Biomedical Engineering, Cairo University, Egypt worked as Assistant Professor at MTI University.

Dr. Aurora Angela Pisano

Ph.D. in Civil Engineering, Currently Serving as Associate Professor of Solid and Structural Mechanics (scientific discipline area nationally denoted as ICAR/08"–"Scienza delle Costruzioni"), University Mediterranea of Reggio Calabria, Italy.

Dr. Faizullah Mahar

Associate Professor in Department of Electrical Engineering, Balochistan University Engineering & Technology Khuzdar. He is PhD (Electronic Engineering) from IQRA University, Defense View, Karachi, Pakistan.

Prof. Viviane Barrozo da Silva

Graduated in Physics from the Federal University of Paraná (1997), graduated in Electrical Engineering from the Federal University of Rio Grande do Sul - UFRGS (2008), and master's degree in Physics from the Federal University of Rio Grande do Sul (2001).

Dr. S. Kannadhasan

Ph.D (Smart Antennas), M.E (Communication Systems), M.B.A (Human Resources).

Dr. Christo Ananth

Ph.D. Co-operative Networks, M.E. Applied Electronics, B.E Electronics & Communication Engineering Working as Associate Professor, Lecturer and Faculty Advisor/ Department of Electronics & Communication Engineering in Francis Xavier Engineering College, Tirunelveli.

Dr. S.R.Boselin Prabhu

Ph.D, Wireless Sensor Networks, M.E. Network Engineering, Excellent Professional Achievement Award Winner from Society of Professional Engineers Biography Included in Marquis Who's Who in the World (Academic Year 2015 and 2016). Currently Serving as Assistant Professor in the department of ECE in SVS College of Engineering, Coimbatore.

Dr. PAUL P MATHAI

Dr. Paul P Mathai received his Bachelor's degree in Computer Science and Engineering from University of Madras, India. Then he obtained his Master's degree in Computer and Information Technology from Manonmanium Sundaranar University, India. In 2018, he received his Doctor of Philosophy in Computer Science and Engineering from Noorul Islam Centre for Higher Education, Kanyakumari, India.

Dr. M. Ramesh Kumar

Ph.D (Computer Science and Engineering), M.E (Computer Science and Engineering).

Currently working as Associate Professor in VSB College of Engineering Technical Campus, Coimbatore.

Dr. Maheshwar Shrestha

Postdoctoral Research Fellow in DEPT. OF ELE ENGG & COMP SCI, SDSU, Brookings, SD Ph.D, M.Sc. in Electrical Engineering from SOUTH DAKOTA STATE UNIVERSITY, Brookings, SD.

Dr. D. Amaranatha Reddy

Ph.D. (Postdocteral Fellow, Pusan National University, South Korea), M.Sc., B.Sc. : Physics.

Dr. Dibya Prakash Rai

Post Doctoral Fellow (PDF), M.Sc., B.Sc., Working as Assistant Professor in Department of Physics in Pachhuncga University College, Mizoram, India.

Dr. Pankaj Kumar Pal

Ph.D R/S, ECE Deptt., IIT-Roorkee.

Dr. P. Thangam

PhD in Information & Communication Engineering, ME (CSE), BE (Computer Hardware & Software), currently serving as Associate Professor in the Department of Computer Science and Engineering of Coimbatore Institute of Engineering and Technology.

Dr. Pradeep K. Sharma

PhD., M.Phil, M.Sc, B.Sc, in Physics, MBA in System Management, Presently working as Provost and Associate Professor & Head of Department for Physics in University of Engineering & Management, Jaipur.

Dr. R. Devi Priya

Ph.D (CSE), Anna University Chennai in 2013, M.E, B.E (CSE) from Kongu Engineering College, currently working in the Department of Computer Science and Engineering in Kongu Engineering College, Tamil Nadu, India.

Dr. Sandeep

Post-doctoral fellow, Principal Investigator, Young Scientist Scheme Project (DST-SERB), Department of Physics, Mizoram University, Aizawl Mizoram, India- 796001.

Dr. Roberto Volpe

Faculty of Engineering and Architecture, Università degli Studi di Enna "Kore", Cittadella Universitaria, 94100 – Enna (IT).

Dr. S. Kannadhasan

Ph.D (Smart Antennas), M.E (Communication Systems), M.B.A (Human Resources).

Research Area: Engineering Physics, Electromagnetic Field Theory, Electronic Material and Processes, Wireless Communications.

Mr. Amit Kumar

Amit Kumar is associated as a Researcher with the Department of Computer Science, College of Information Science and Technology, Nanjing Forestry University, Nanjing, China since 2009. He is working as a State Representative (HP), Spoken Tutorial Project, IIT Bombay promoting and integrating ICT in Literacy through Free and Open Source Software under National Mission on Education through ICT (NMEICT) of MHRD, Govt. of India; in the state of Himachal Pradesh, India.

Mr. Tanvir Singh

Tanvir Singh is acting as Outreach Officer (Punjab and J&K) for MHRD Govt. of India Project: Spoken Tutorial - IIT Bombay fostering IT Literacy through Open Source Technology under National Mission on Education through ICT (NMEICT). He is also acting as Research Associate since 2010 with Nanjing Forestry University, Nanjing, Jiangsu, China in the field of Social and Environmental Sustainability.

Mr. Abilash

MTech in VLSI, BTech in Electronics & Telecommunication engineering through A.M.I.E.T.E from Central Electronics Engineering Research Institute (C.E.E.R.I) Pilani, Industrial Electronics from ATI-EPI Hyderabad, IEEE course in Mechatronics, CSHAM from Birla Institute Of Professional Studies.

Mr. Varun Shukla

M.Tech in ECE from RGPV (Awarded with silver Medal By President of India), Assistant Professor, Dept. of ECE, PSIT, Kanpur.

Mr. Shrikant Harle

Presently working as a Assistant Professor in Civil Engineering field of Prof. Ram Meghe College of Engineering and Management, Amravati. He was Senior Design Engineer (Larsen & Toubro Limited, India).

Zairi Ismael Rizman

Senior Lecturer, Faculty of Electrical Engineering, Universiti Teknologi MARA (UiTM) (Terengganu) Malaysia Master (Science) in Microelectronics (2005), Universiti Kebangsaan Malaysia (UKM), Malaysia. Bachelor (Hons.) and Diploma in Electrical Engineering (Communication) (2002), UiTM Shah Alam, Malaysia.

Mr. Ronak

Qualification: M.Tech. in Mechanical Engineering (CAD/CAM), B.E.

Presently working as a Assistant Professor in Mechanical Engineering in ITM Vocational University, Vadodara. Mr. Ronak also worked as Design Engineer at Finstern Engineering Private Limited, Makarpura, Vadodara.

Table of Contents

Volume-10, Issue-10, October 2024

Design of Hydroponic System Plant Growing with Automatic Control

Romana Dobáková[1*]; Natália Jasminská[2]; Ivan Mihálik[3]

Department of Energy Engineering, Faculty of Mechanical Engineering, Technical University of Košice, Slovakia
*Corresponding Author

Received: 26 September 2024/ Revised: 08 October 2024/ Accepted: 14 October 2024/ Published: 31-10-2024

Abstract— *Rapid urbanization and industrialization cause not only the reduction of agriculturally usable areas, but also a certain degree of modification of traditional cultivation practices. Cultivation of plants with the use of new technologies, characterized by the absence of land use, is experiencing significant development in areas of unconventional agriculture, primarily in areas with a lack of land or unsuitable soil quality. The article discusses the design of an island system for local year-round production of seasonal food using an alternative source of energy. The output is the design of your own hydroponic system with automatic control.*

Keywords— Hydroponics, Plants, Island System.

I. INTRODUCTION

Due to the constant increase in the number of people on our planet, the need for food and water is a fundamental problem for humanity. Another serious problem is the uncontrollable pollution of the planet and the associated loss of quality agricultural land. In many areas of the Earth there is a shortage of drinking water or environment unsuitable for growing plants. For this reason, hydroponic systems can provide a suitable environment for growing food while managing natural resources efficiently. The first large-scale experiments using hydroponic cultivation come from German botanists from the second half of the 19th century. One of the first successes of hydroponics occurred on Wake Island, a rocky atoll in the Pacific Ocean used as a refuelling stop for Pan American Airlines. Hydroponics was used there in the 1930s to grow vegetables for passengers. This method of cultivation was a necessity on Wake Island because there was no suitable land for growing the desired types of plants and the transportation of fresh vegetables by air was prohibitively expensive. In recent decades, NASA has conducted extensive hydroponic research on its Controlled Ecological Life Support System (CELSS). This research, mimicking the Martian environment, uses LED lighting to grow in a different colour spectrum with much less heat.

II. HYDROPONIC SYSTEMS

Hydroponics is one of the most modern methods of growing plants indoors. A characteristic feature of this method is growing plants in a nutrient medium without soil (Fig. 1). Hydroponic cultivation ensures optimal, almost natural conditions for growth and development, a certain degree of protection against diseases and at the same time a hygienic environment for plants, as the soil represents a potential source of various diseases, parasites and parasitic plants.

According to the distribution of the nutrient solution, hydroponic systems can be divided into closed and open. The closed system is characterized by feeding the nutrient solution to the plants in specially constructed cultivation troughs. The main advantage of this system is that the solution circulates and is fed back to the plants, which increases the extraction of the nutrients necessary for growth contained in the nutrient solution. Conversely, the primary disadvantage of nutrient solution recirculation can be the transmission of root diseases, which, however, poses a minimal risk under indoor conditions. The division of hydroponic systems according to the substrate and according to the environment that will be created around the root system is most often used. From this point of view, we distinguish between water, substrate and air cultures. Aquatic cultures have a closed circuit of nutrient solution distribution, plant roots are directly surrounded by it. A significant advance in the application of water cultures is the NFT (Nutrient Film Technique) system (Fig. 2), where the nutrient solution continuously flows through the bottom of the growing container, washes the roots in a thin layer (1-2 cm) and then returns to the storage tank.

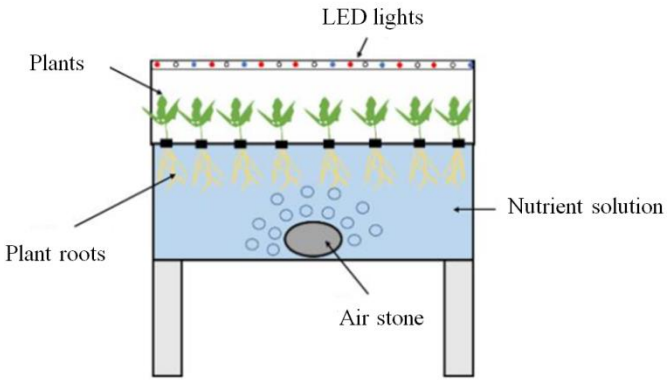

FIGURE 1: Hydroponics [1]

Plants have enough air. The second important system based on water culture is the DFT (Deep Flow Technique) system (Fig. 3), which is characterized by growing plants floating or hanging on supports (rafts, boards, panels) in containers filled with a nutrient solution.

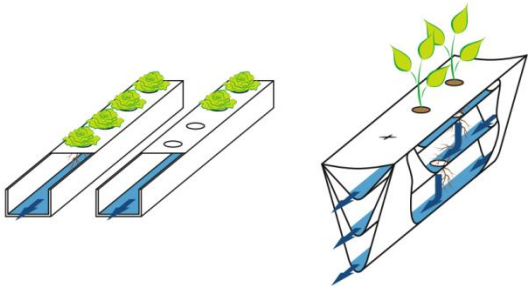

FIGURE 2: NFT system: single-layer trough (left), multi-layer trough (right)

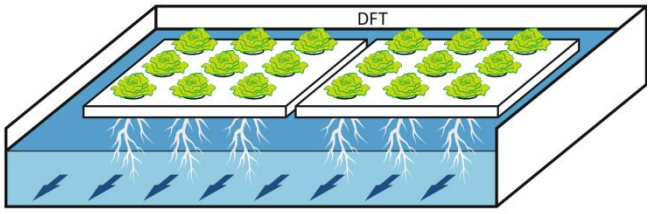

FIGURE 3: DFT system

Air culture, or aeroponics (Fig.4) is a soilless technology, which is characterized by the placement of plant roots in a closed device, while they are moistened with a nutrient solution at short intervals or continuously using a spray nozzle, which is placed under the plant root. In the aeroponic system, the plant grows in the air with the help of artificial support. Substrate culture is mostly used in interiors. Crops are grown in a solid, indoor non-inert medium instead of soil or water. As a medium for root systems, it uses substrates that are inert to chemicals, plant activity and microbial activity (e.g. inorganic substrates: coarser siliceous sand, inert volcanic tuffs, perlite, zeolite, gravel, stone wool, pumice, sepiolite, expanded clay, organic substrates: peat, conifer bark, wood chips). An effective substrate material must have a physical structure that creates an appropriate balance of air and water for healthy root development.

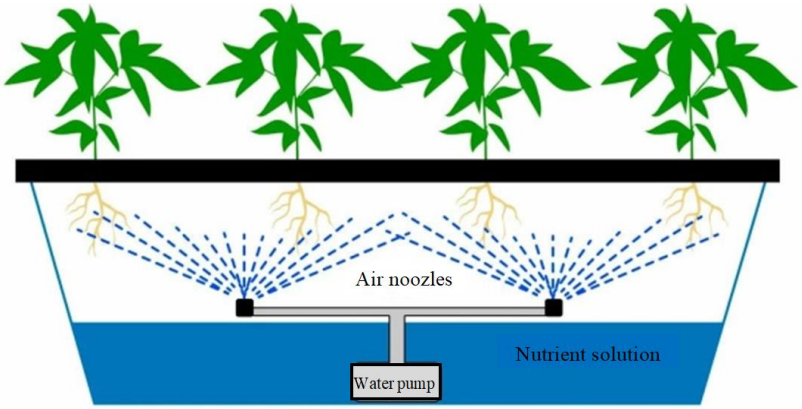

FIGURE 4: Air culture

Many plants, various crops and vegetables can be grown using hydroponic systems. The taste, nutritional value of the final products and their quality are generally higher compared to conventional soil cultivation. Experimental findings point to the possibility of successfully growing leafy vegetables (spinach, lettuce, parsley, celery, etc.) using hydroponics.

III. DESIGN OF AN ISLAND SYSTEM WITH THE POSSIBILITY OF YEAR-ROUND CULTIVATION OF SELECTED CROP TYPES

The implementation and operation of the island system for local year-round production of seasonal food is directly dependent on several aspects. It is possible to include the selected type of cultivated crop, its nutritional and light requirements, the need to maintain a suitable interior temperature, etc. When designing the island system, the NFT hydroponic system was chosen. The proposed system consists of the following components: growing unit, hydroponic system components (tanks, pumps, hoses, growing grids, air stones, etc.), growing medium, nutrient solution, ventilation system, temperature management system, software-hardware management equipment systems, pH and EC (electrical conductivity) meters, additional grow lights (LED, high-pressure sodium, etc.), backup source based on LiFePO4 battery pack, photovoltaic panels.

A shipping container 20 with internal dimensions of 5910x2345x2690 mm was designed as a growing unit. The container was insulated from the inside with glass wool and OSB boards. A container with a volume of 100 l was chosen for storing and supplying the plants with nutrient solution, which was placed in the corner of the container. Inside the container there is an air stone (diameter 150 mm and thickness 18 mm), which serves to aerate the nutrient solution, and thus ensures the distribution of oxygen to the cultivated plants. It is connected to a compressor pumping air from inside the container to bring it to the storage tank. The air stone divides the air flow into microbubbles, from which oxygen dissolves more easily in the water. The distribution of the nutrient solution by the hydroponic system is provided by a circulating pump (power 0.071 kW, maximum flow 55 $l \cdot min^{-1}$). Part of the designed system is also a hybrid air conditioning unit serving to reduce the system's energy requirements and ensure financial efficiency. Part of the designed system is also a hybrid air conditioning unit serving to reduce the system's energy requirements and ensure financial efficiency. To ensure the independent operation of the hydroponic system in the form of an island operation, photovoltaic panels (18 pcs., each with a maximum power of 500W) were chosen, which ensure the operation of the entire system and at the same time serve to recharge the batteries. The proposed accumulators are supposed to ensure the coverage of the energy requirements of the island system even when the photovoltaic panels do not supply the required electrical power. The hydroponic system was made of PVC pipes, where mesh cups were inserted into the drilled holes. Holes for supply and drain hoses were created in the PVC pipes. The pipe system was placed on a stand that considered the appropriate spacing of the pipes connected by means of clamps depending on the plant being grown. An LED strip with adjustable colour and intensity of radiation was chosen as a substitute for natural light for growing plants. An EC meter was used to measure conductivity in the nutrient solution, and a pH meter was used to measure its alkalinity. Mineral wool was used as a growing medium. In the given island system, the cultivation of leafy vegetables is ensured with the help of hydroponics.

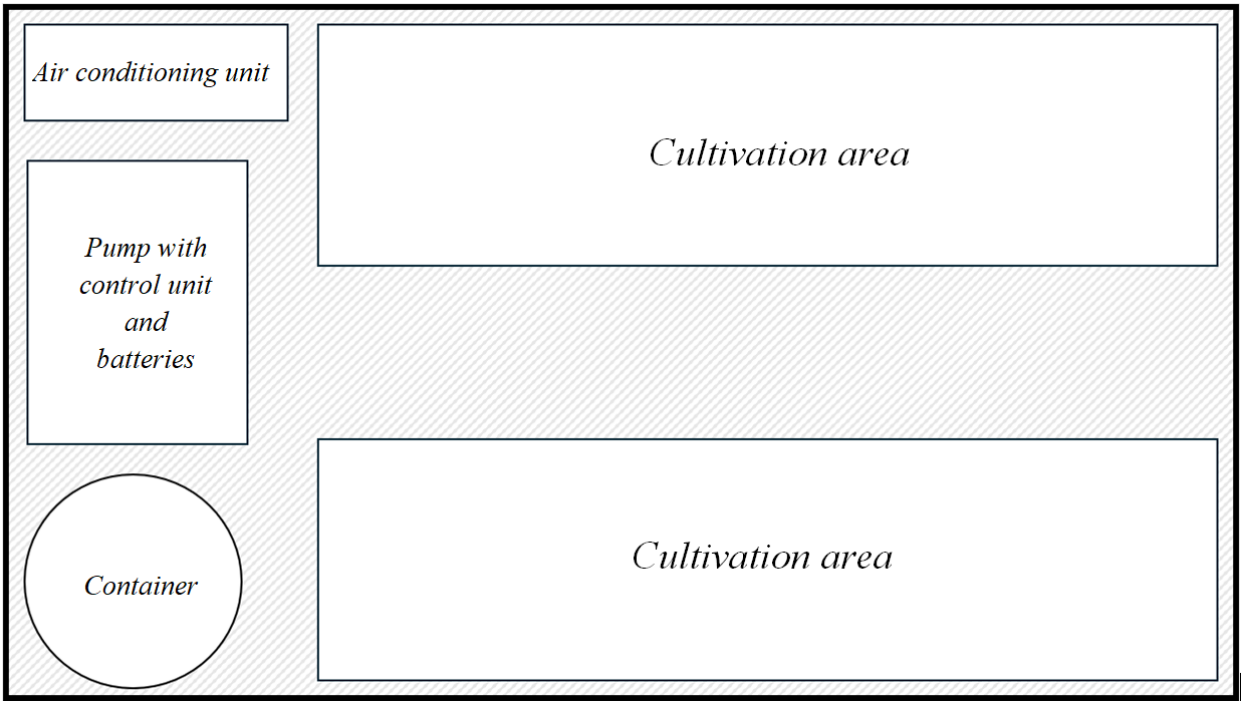

FIGURE 5: Scheme of the shipping container equipment

To ensure appropriate management of temperature, amount of nutrients and lighting intensity according to the requirements of individual plant species and according to their level of development, a Raspberry Pi 4 microcomputer was chosen. The use of microcomputers ensures a reduction in energy requirements for the control unit and at the same time enables remote access to ensure regular monitoring required parameters without the need for physical presence. Sensors monitoring the basic values of the nutrient solution using EC and pH probes, the temperature of the solution, the flow of the solution through the cultivation device and the possible occurrence of unwanted algae using optical sensors are connected to the microcomputer system. The system also monitors the level of the nutrient solution in the container and, in the event of a sharp drop, ensures the closure of the entire system and reports a malfunction. To add nutrients to the main tank, a tank with nutrients is connected to it using a small pump, which is controlled by a microcomputer, and in the event of a decrease in nutrients in the main tank, they are automatically replenished. Sensing the amount of nutrients in the main container was chosen with regard to easier controllability of their amount. The system also monitors the amount of nutrients at the exit from the growing part for the analysis of the consumption of the nutrient medium in individual parts of the vegetation cycle of the cultivated plants.

Fig. 6 shows the resulting design of an island system for local year-round production of seasonal food capable of producing approx. 1680 pieces of leafy vegetables.

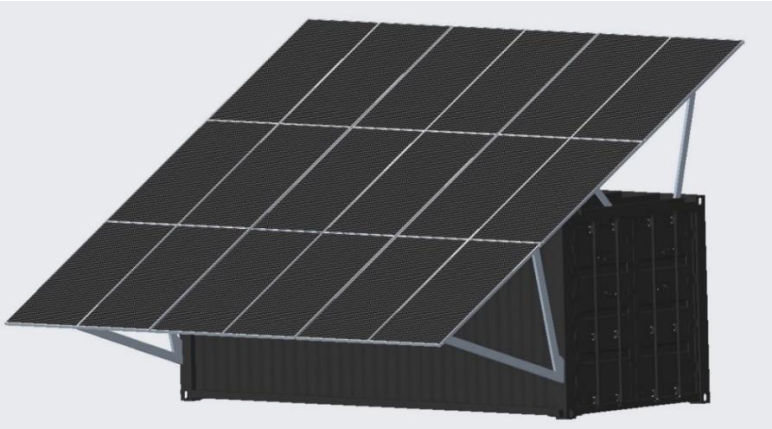

FIGURE 6: Container model

The hydroponic growing system requires the maintenance of stable operating conditions during the entire working cycle regardless of external conditions. To ensure the required operational parameters, it was necessary to propose the necessary structural modifications, which include the insulation of the transport container, the installation of the energy system and temperature management. The temperature management system was designed with heat gains and losses in mind throughout the year. With the changing external temperature, there is also a change in the demands on temperature management, primarily on its performance, with the aim of maintaining an interior temperature of 25 °C. Performance requirements, whether for heating or cooling throughout the year, are shown in table 1.

TABLE 1
PERFORMANCE REQUIREMENTS OF A HYDROPONIC SYSTEM

Outside temperature (°C)	Required heat output to maintain stable internal conditions (25°C) (kW)	Intensity of air exchange in the container (h^{-1})	Evaluation of performance requirements
-30	5.88	0.5	Heat up
-6	3.49	1	Heat up
-3	3.15	1	Heat up
5	2.24	1	Heat up
8.5	1.85	1	Heat up
15	1.11	1	Heat up
18.5	0.72	1	Heat up
40	1.63	0.5	Cool down

The required heat output for maintaining stable internal conditions was calculated according to the STN EN 128 31-1 standard for the Košice location.

For the need to cover the energy self-sufficiency of thermal management and associated systems for hydroponic cultivation, a photovoltaic system installed on a steel structure placed on a container according to fig. 6. The angle of inclination of the panels is 30°, while their secondary function is the screening of the container itself. Shading the container ensures protection against overheating due to direct sunlight, which would increase the energy requirements for cooling during the hottest months of the year. The total installed power of the photovoltaic system is 9 kW. The hydroponic system is in Košice, which is essential information for considering the daylight hours to calculate the amount of energy produced by the photovoltaic panels. With 14 hours of sunlight, the system can produce 126 kWh of electricity through 18 photovoltaic panels.

Thermal management consumption is defined as variable, while hydroponic growing system consumption is constant. Instability in the amount of incident solar radiation, primarily during the winter period, has the task of compensating the designed battery systems, consisting of LiFePO4 batteries. They use the free space in the shipping container, where it is not possible to directly install any technology or cultivation equipment. The chosen number of batteries is 33, which represents storage for 84.48 kW of electricity. The water contained in the hydroponic system also serves as a temperature stabilization medium. The total volume of water exceeds 195 l, which creates a storage source of thermal energy. It serves to stabilize the internal operating conditions in the transport container for hydroponic crop cultivation. In case of deterioration of external conditions, thanks to microcomputer control, it is possible to adjust the energy consumption of the entire system in such a way that cultivated plants are protected for a longer period from the effects of the external cold environment. Such interventions include limiting the exchange of air with the external environment, reducing the temperature in the growing environment to 10 °C, which will decrease the energy requirements for heating, as well as reducing the exposure time of the plants and the operating time of the circulation pumps. The main reason for the deterioration of external conditions in winter is the covering of photovoltaic panels with a layer of snow or frost, or a long-term reduced supply of solar radiation caused by unfavourable meteorological conditions.

IV. CONCLUSION

The biggest benefit of hydroponics is growing plants without using soil. Thanks to this, plants can be grown even in an otherwise unfavourable environment, many times even with extreme conditions. From the point of view of huge saving of area, hydroponics can be used even in urban areas for vertical cultivation. The proposed modular island system represents a self-sufficient local year-round production of seasonal food, as it uses photovoltaic panels with a set of appropriately selected batteries to ensure the necessary operating conditions. The modularity of the container enables the system's exploitability to be increased by increasing the number of connected units without the need for drastic intervention in individual modules. The primary purpose of the article is an attempt to describe the possibilities of applying container plant growing systems even in areas of urban urbanization without the need for significant interventions in the environment. The article is the initial phase of research into the applicability of hydroponic growing systems in unused industrial and commercial spaces within the territory of the Slovak Republic and the surrounding area.

ACKNOWLEDGEMENTS

This paper was written with the financial support from the KEGA granting agency within the Project No. 012TUKE-4/2022.

REFERENCES

[1] Lakhiar, I. A., et al.: *Overview of the aeroponic agriculture –An emerging technology for global food security*. Int J Agric & Biol Eng., 13 (1) 2020, p. 2–10.

[2] Feriancová, Ľ.: *Hydroponics – New Technology of Cultivating Indoor Plants*. Život. Prostr., 38 (1) 2004, p. 40 – 43.

[3] Frasetya, B., K Harisman, K., Ramdaniah, H.: *The effect of hydroponics systems on the growth of lettuce*. IOP Conf. Series: Materials Science and Engineering, 1098 (2021) 042115.

[4] Sharma, N., et al.: *Hydroponics as an advanced technique for vegetable production: An overview*. Journal of Soil and Water Conservation, 17(4) 2018, p. 364–371.

[5] Dominques, D., et al.: *Automated system developed to control pH and concentration of nutrient solution evaluated in hydroponic lettuce production.* Computers and Electronics in Agriculture, 84 2012, p. 53–61.

Theoretical Analysis of the Natural Separation of Hydrogen and Natural Gas in the Pipelines of An Apartment Building

Romana Dobáková[1*]; Natália Jasminská[2]; Marián Lázár[3]

Department of Energy Engineering, Faculty of Mechanical Engineering, Technical University of Košice, Slovakia
*Corresponding Author

Received: 28 September 2024/ Revised: 09 October 2024/ Accepted: 16 October 2024/ Published: 31-10-2024

Abstract— *Due to the current development of the state of fossil resources, efforts are being made to replace extractable energy sources with renewable sources that would have less impact on the environment during the production, transport and consumption processes. Hydrogen is a promising universal energy carrier that could gradually replace the currently used fossil fuels to a large extent. The article discusses the problem of mixing hydrogen into natural gas using simulation in the ANSYS CFX program into the proposed distribution network, as well as its behaviour in a mixture with natural gas in the case of reduced consumption by the consumer, or during downtime or repairs, when the flow in the intake pipe is reduced or completely stopped.*

Keywords— ANSYS CFX, hydrogen, natural gas.

I. INTRODUCTION

Fossil fuels are found in nature only in limited quantities, and with today's dependence of humanity on their excessive use, it can be assumed that within the horizon of several decades, society will reach a point when the reserves of these energy sources will reach a critical point and demand for them will exceed production.

Experiments are currently taking place that deal with the use of the already existing distribution network for the implementation of hydrogen economy in current gas systems and explore the possibilities of transporting hydrogen to the final consumer without the need for significant technological interventions in the natural gas distribution network (ZP). In many countries, the process of mixing different proportions of hydrogen into natural gas is already underway to achieve a reduction in the production of greenhouse gases, and research is also underway into the behaviour of the mixture of hydrogen and natural gas during transport in the pipeline network.

II. MIXING HYDROGEN INTO NATURAL GAS

In addition to high potential, the use of hydrogen hides the need for a total change in infrastructure. Among other things, technical, economic and institutional changes are needed to create a full hydrogen economy, the implementation of which may take decades. These changes concern all individual segments of the energy system, namely production, distribution, storage and use by end consumers. For end users, measures are required due to the change in the properties of the burned mixture of hydrogen and natural gas, considering aspects such as backflow, unintended gas release, efficiency, service life and safety of gas appliances. Among other things, hydrogen can also affect the material properties of the pipeline system, which have an impact on overall safety.

The service life of some types of pipes can be reduced if they are exposed to hydrogen for a long time, especially at higher concentrations and at high pressures. Hydrogen can cause damage to steel pipes even under normal operating conditions in natural gas distribution systems. Hydrogen encounters the pipe material, diffuses through the structure of this material, causes its embrittlement and subsequent degradation of its mechanical properties and the formation of microcracks.

The advantage of mixing hydrogen into natural gas is a significant reduction in greenhouse gas emissions, provided that the hydrogen is produced from low-carbon energy sources, for example using solar, wind, nuclear energy or from fossil energy

sources with carbon capture and storage. Mixing hydrogen into natural gas improves air quality in urban areas by reducing the amount of sulphur dioxide and carbon dioxide produced during the natural gas combustion process.

When hydrogen is mixed with natural gas, similarly to when other gases of different densities are mixed, a phenomenon called stratification of the gas mixture can occur. In such a case, different vertical layers of these gases with different representation of individual components may occur in the pipeline, in which there are gases with different densities. A gas with a lower bulk density rises compared to a gas with a higher bulk density. In addition to the influence of gravity on the separation capabilities of gases with different densities, diffusion acts in a mixture of two or more gases. Thanks to the free movement of particles in the pipe, the gases diffuse each other, and thus, under ideal conditions, a homogeneous mixture is created. For low mixture flow conditions that raise concerns about imperfect mixing, injection methods are used to maximize mixing.

III. THE EFFECT OF HYDROGEN ON THE SAFETY OF HOUSEHOLD APPLIANCES

To be able to replace todays commonly used natural gas with a mixture of natural gas and hydrogen in household appliances, the condition of the possibility of safe combustion without the need for structural modifications of the appliances must be met. If it were not possible to burn such a gaseous mixture in already existing facilities, it would mean extensive costs for modification or replacement of appliances for many households.

At the same time, there is a general agreement in publications of renowned companies that a hydrogen content of up to 10% does not represent any or negligible technical risk for existing household appliances [1].

Mixing hydrogen into the mixture with natural gas affects the performance of the burner or power consumption of the appliance, as the combustion heat and calorific value of the given mixture decreases with the increasing proportion of hydrogen in the mixture, and when the pressure parameters of the mixture are maintained, it causes a decrease in the performance of the burners and thus also the power consumption of the appliance. The increasing amount of hydrogen causes a decrease in the density of the entire mixture and, consequently, an increase in the flow rate and thus the amount of mixture flowing through the burner nozzle.

When burning mixtures of natural gas with hydrogen, the values of adiabatic temperatures and actual combustion temperatures in the burners of household appliances are higher than in the case of burning pure natural gas, because hydrogen has higher combustion temperatures than natural gas under the same combustion conditions. Since the combustion of a mixture of natural gas and hydrogen leads to an increase in the stoichiometric volume of the combustion air and thus to a decrease in the temperature of the flue gases, an increase in the combustion temperatures of mixtures of natural gas and hydrogen should not have any effect on the functionality of domestic gas appliances [1].

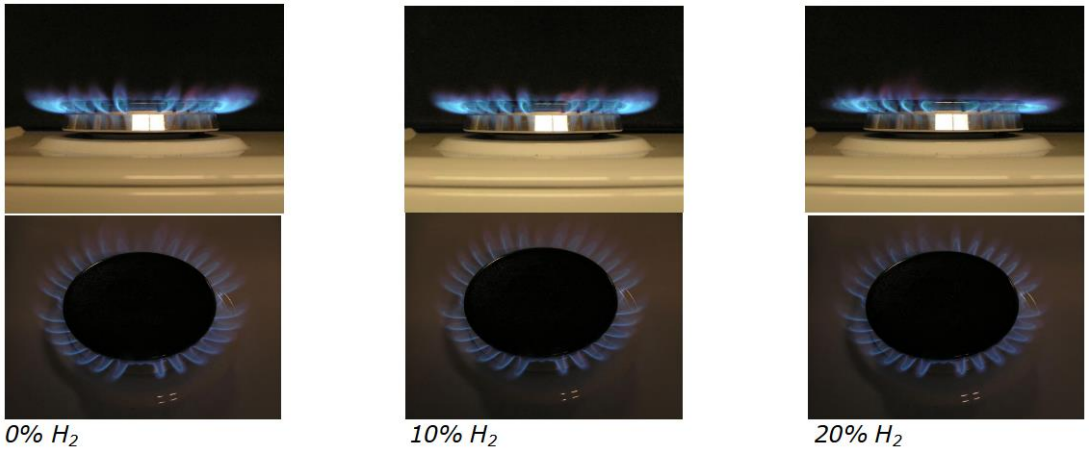

FIGURE 1: Flame from the burner of a gas appliance at different proportions of hydrogen mixed with natural gas [2]

When mixing hydrogen into a mixture with natural gas, it is necessary to assess its impact on safety in the event of its leakage, either in the event of an accident of the given gas equipment or during a long-term shutdown of the equipment using the combustion of the natural gas mixture treated in this way. Hydrogen is generally easily flammable and therefore when it escapes from the pipe or there is a risk of ignition from the device under pressure due to the turbulent mixing of hydrogen and the surrounding air.

IV. BOUNDARY CONDITIONS FOR SIMULATION IN PROGRAM ANSYS CFX

In order to assess the behavior of hydrogen in a mixture with natural gas, a simulation was carried out in the ANSYS CFX program in the proportional representation of 20% hydrogen and 80% methane. The selected pipe section on which the simulation took place represents the main pipe with four sampling points in a four-story apartment building, where gas was used only for cooking. There was one collection point on each floor. The distance of the sampling points from the main vertical pipeline is 1000 mm, and the distance between the individual floors on which the sampling points are located is 2500 mm. The diameter of the main pipe located vertically is 56 mm, and the diameter of the supply pipes to the gas measuring devices is 32 mm. The inlet of the gas mixture to the pipeline system is located at the lowest point set as OPENNING with the relative pressure at the inlet set to 0 Pa (fig.2).

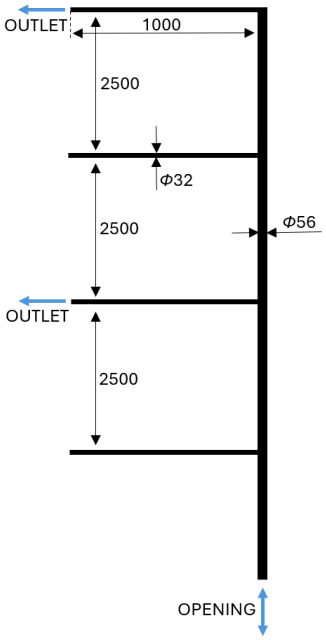

FIGURE 2: Location of individual collection points in a four-story apartment building

Solving the problem of the behaviour of hydrogen in a mixture with natural gas was carried out under two boundary conditions. In the first case, there was no sampling from the main pipeline at any sampling point. This variant represents a period of inactivity during the night hours or during periods with reduced consumption of natural gas, or shutdowns. Assessing the behaviour of hydrogen in a mixture with natural gas at zero consumption is important, as due to their different densities, hydrogen tends to separate from the rest of the mixture. The accumulation of hydrogen in the upper layers of the pipeline during long-term shutdowns can cause undesirable circumstances, such as hydrogen leakage, which can be difficult to detect, since hydrogen is not odorized, or a decrease in the mechanical properties of the pipelines. In the second assessed state, the sampling was realized only on the fourth and second floors, on the remaining two floors the sampling was zero, as shown in fig. 2. Subsequently, the intake of the gas mixture was closed on the highest floor and, after a time interval of 5 minutes, also on the second floor. In the case of consumption, the proposed maximum consumption of a gas stove when using four burners is 2.13 $m^3 \cdot h^{-1}$. Initialization conditions are set to 0 Pa overpressure. After the implementation of the active gas mixture extraction, the simulation time of zero extraction was chosen to be 8 hours, which represents approximately the time of night rest.

In both cases, the development of the distribution of the gas mixture in the pipeline system as well as the possible stratification of individual components along the pipeline height are subsequently investigated.

V. EVALUATION OF THE EXPERIMENT USING SIMULATION IN THE ANSYS CFX

The results of the simulation experiment show the possible probability of the formation of a layer of highly concentrated hydrogen in a mixture with a small proportion of methane in the highest parts of the pipeline distribution system. With increasing time at zero flow in the supply horizontal pipelines to the sampling point of the gas mixture, it is possible to observe a gradual increase in the proportion of hydrogen in the mixture at the expense of the proportion of methane. The longer the

shutdown of the gas mixture intake, the larger the area with the increased proportion of hydrogen. The formation of areas can be observed at the highest points of the distribution pipeline system (fig.3, 4).

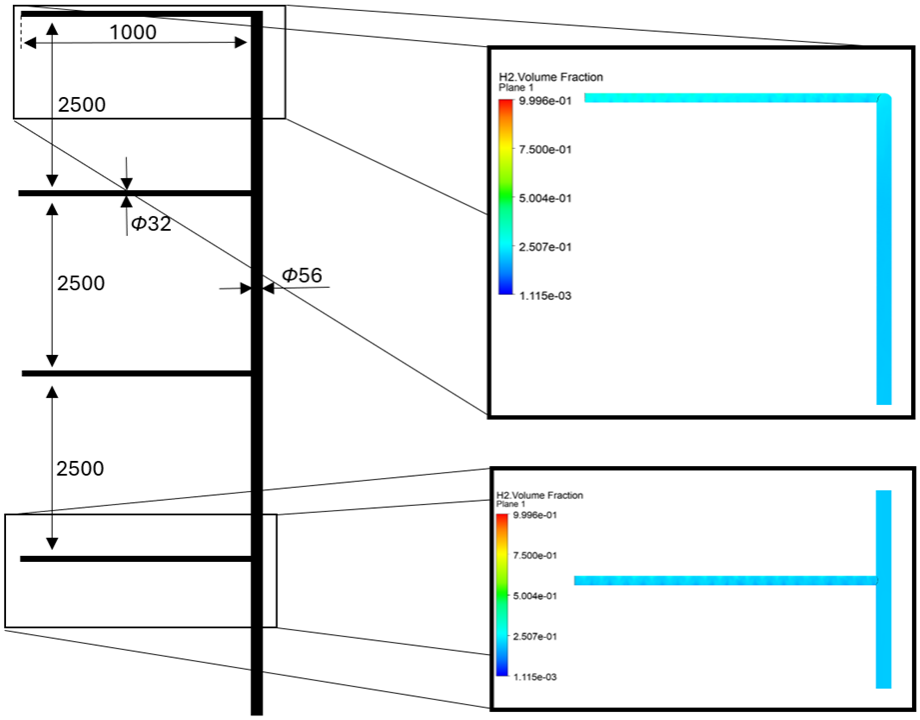

FIGURE 3: Distribution of hydrogen concentration in the distribution system after 2 hours

The separation of hydrogen from natural gas occurred in approximately the same way in the case of the simulation with and without withdrawal. After a period of approx. 15 minutes from the stop of withdrawals, the course of the simulation was roughly the same. In fig. 3 shows the state after two hours from the closing of the withdrawals. It is possible to observe the gradual increase of the hydrogen concentration in the highest intake pipe. The total concentration of hydrogen in this pipeline was around 25-30%.

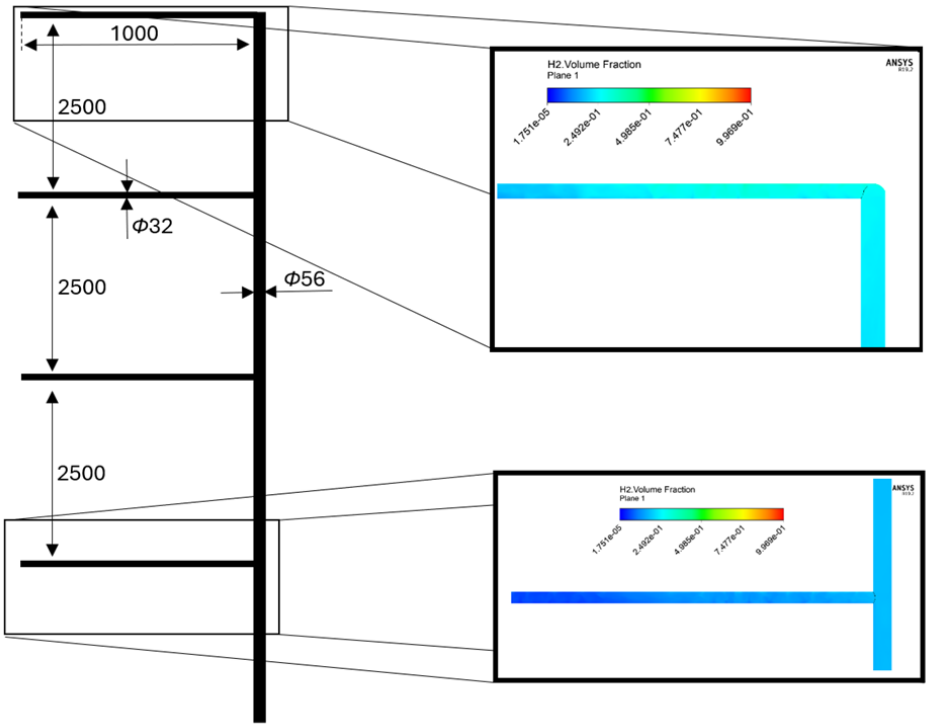

FIGURE 4: Distribution of hydrogen concentration in the distribution system after 8 hours

If the gas withdrawal period exceeds a certain critical time limit, a continuous layer of hydrogen may form, as can be seen in fig. 4. In the case of a longer shutdown of appliances in the highest levels of the distribution of the gas mixture, which may be caused by the non-occupancy of the premises, or the holiday season, the layer of hydrogen in the gas distribution can reach a height of several meters. Such a phenomenon can occur because of the constant supply of fresh gas mixture due to the use of gas appliances in the lower levels of the distribution system and subsequent shutdowns during the night.

Due to the influence of diffusion, continuous mixing of hydrogen with natural gas occurs within the vertical pipeline, but the diameter of the intake horizontal pipes probably impairs the ability of hydrogen to diffuse into the natural gas, resulting in its gradual separation. Despite diffusion, hydrogen is gradually transported to higher parts of the pipeline distribution system. In fig. 4 it is possible to observe that hydrogen concentrations locally reached a limit exceeding 35-40%. At the same time, it is possible to observe that the concentration of hydrogen in the lowest horizontal pipe dropped significantly below the 20% limit. The local increase in hydrogen concentration in the pipeline is primarily influenced by time and mainly by the total amount of hydrogen present in the distribution pipeline system. In places with an increased concentration of hydrogen, damage to distribution systems can occur due to hydrogen embrittlement.

VI. CONCLUSION

Even though the results of simulation experiments cannot be considered as accurately describing the processes that take place in gas pipelines for the distribution of a mixture of natural gas and hydrogen, it would be appropriate to focus on the experimental solution of the problem described in of this article. The formation of areas with a significant presence of hydrogen in the mixture in the pipeline system ensuring the transport of such a mixture can mean a potential danger in case of stoppages of gas mixture intakes.

From the simulation experiments, it is possible to assume the formation of layers with an increased concentration of hydrogen in both horizontal and vertical pipelines, while the probability of the formation of such zones with a higher concentration of hydrogen also increases with increasing height within the distribution system of a mixture of hydrogen with natural gas.

ACKNOWLEDGEMENTS

This paper was written with the financial support from the VEGA granting agency within the Projects No. 1/0224/23 and No. 1/0532/22, from the KEGA granting agency within the Project No. 012TUKE-4/2022, and with the financial support from the APVV granting agency within the Projects No. APVV-21-0274 and APVV- 23-0266.

REFERENCES

[1] SIEA: *Využitie vodíka v spotrebičoch na zemný plyn pre domácnosť.* Available on: <www.siea.sk >.

[2] Kippers,M.J., De Laat, J.C., Hermekens R.J.M.: *Pilot project on Hydrogen injection in natural gas on Island of ameland in the Netherlands.* International Gas Union Research Conference, 2011

[3] Zabrzeski, L., Janusz, P., Liszka, K., Laciak, M., SZulej, A., *Hydrogen-Natural Gas mixture compression in case of transporting through high-pressure gas pipelines*, Conf. Ser.: EarthEnviron. Sci. 214, 012137

[4] Gondal, I.A.: *Hydrogen integration in power-to-gas networks.* International Journal of Hydrogen Energy. Vol. 44 (3), pp. 1803-1815.

[5] Santoli, L., Lo, B.G., Nastasi, B.: *The potential of hydrogen enriched natural gas deriving from power-to-gas option in building energy retrofitting*. Energy Build, 149 (2017), pp. 424-436.

[6] Atfeld, K., Pinchbek D.: *Admissible hydrogen concentrations in natural gas systems*. Gas for energy 03(2013), pp. 1-12.

Hybrid Strategy improves Crayfish Optimization Algorithm

Tong Ding

School of Big Data and Statistics, Guizhou University of Finance and Economics, Guiyang, Guizhou Province

Received: 01 October 2024/ Revised: 11 October 2024/ Accepted: 18 October 2024/ Published: 31-10-2024

Abstract— *In response to the deficiencies of the Crayfish Optimization Algorithm (COA), such as slow convergence speed and susceptibility to local optima when solving complex optimization problems, an improved Crayfish Optimization Algorithm (ICOA) with a hybrid strategy is proposed. This improvement incorporates five strategies: an enhanced position update function for followers from the Sparrow Algorithm, a refined spiral position update function from the Whale Optimization Algorithm, modifications to the criteria and methods for assessing food size, the golden ratio coefficient, and an information accumulation function. Optimization tests conducted on 12 benchmark functions demonstrate that the improved algorithm shows enhancements in both convergence speed and optimization performance. Finally, experiments applying the improved optimization algorithm to engineering application problems further validate the superiority of the enhanced Crayfish Optimization Algorithm.*

Keywords— Classical test functions, COA, Engineering Constraint Problems, Information Accumulation.

I. INTRODUCTION

Traditional optimization algorithms usually target structured problems, which have relatively clear descriptions in terms of the problems and conditions, such as linear programming [1], integer programming [2], mixed programming [3], and constrained or unconstrained conditions [4]. These algorithms possess clear structural information, stable structures and parameters, and unique and clear global optima. Traditional optimization algorithms can be theoretically analyzed in terms of computational complexity and convergence. While they are generally effective for single-extremum problems, they still exhibit many deficiencies when solving multi-extremum problems. In recent years, the increasing complexity of research problems and the ambiguity of computational results have rendered traditional mathematical models increasingly insufficient for these types of problems, creating a growing demand for superior optimization algorithms.

Optimization problems can be expressed as a continuous or combinatorial search space for designs, representing a process of finding the maximum or minimum of a function f(x). The parameter x represents the solution within the search range. The optimization problem goes through multiple iterations to find the optimal solution, ultimately yielding the best solution:

$$x_{best}\left\{x_1, x_2, x_3 \ldots\ldots, x_D\right\}.$$

Here, D denotes the dimensionality of the solution. In each iteration, a new solution

$x_{new}\left\{x_1, x_2, x_3 \ldots\ldots, x_D\right\}$ is generated. If x_{new} is better than x_{best}, then $x_{best} = x_{new}$. The iterations continue until the found solution meets the preset criteria. This final solution (close to the optimal solution) is referred to as the optimal solution. This is the process of meta-heuristic optimization algorithms [5].

Unlike traditional optimization methods, meta-heuristic algorithms do not require consideration of gradient information in the solution space and can search for optimal or suboptimal solutions using random variables and natural heuristic rules[6], [7]. Thus, meta-heuristic algorithms exhibit good resistance to premature convergence, making them easy to program for solving various optimization problems. They have been widely used by scholars in fields such as computer science and medicine (citation). Commonly used meta-heuristic algorithms include the Artificial Bee Colony Algorithm (ABC) [8], Butterfly

Optimization Algorithm (BOA) [9], Grasshopper Optimization Algorithm (GOA) [10], Golden Sine Algorithm (GSA) [11], Moth Flame Optimization Algorithm (MFO) [12], Slime Mold Algorithm (SMA) [13], Teaching-Learning-Based Optimization Algorithm (TLBO)[14], Whale Optimization Algorithm (WOA) [15], and Crayfish Optimization Algorithm (COA)[16], among others. Meta-heuristic algorithms excel in identifying global optimal solutions for optimization problems, and their optimization results are independent of initial conditions while exhibiting strong robustness in the solution domain. As a result, these algorithms have found broad applications in practical scenarios [17][19]. They have demonstrated practical value across various fields, including but not limited to solving the multi-traveling salesman problem [20], multi-level threshold image segmentation [21], ship routing and scheduling problems [22], feature selection [18], [19], and multi-level image segmentation [23]. Currently, scholars have proposed various meta-heuristic algorithms based on characteristics found in nature, which can be broadly categorized into swarm intelligence algorithms, physics-based algorithms, evolutionary algorithms, and human-inspired algorithms [24].

However, according to the no free lunch theorem [25], no single algorithm can solve all optimization problems. Each optimization algorithm is effective for certain optimization problems but ineffective for others. As a result, researchers continuously propose various novel or improved optimization algorithms to address different optimization problems. In 2023, COA introduced a new meta-heuristic optimization algorithm— the Crayfish Optimization Algorithm (COA)— which simulates different strategic behaviors in response to varying environments and food sources. COA presents a method that mimics the foraging, thermoregulating, and competitive behaviors of crayfish. By adjusting temperature, the algorithm balances exploration and exploitation capabilities. However, COA still encounters issues such as slow convergence speed, vulnerability to local optima, and low optimization accuracy. To address these issues, this paper proposes an improved COA operator by integrating an improved position update function from the Sparrow Algorithm, an enhanced spiral position update function from the Whale Optimization Algorithm, the golden ratio coefficient, and an information accumulation function, thereby modifying the factors and methods for assessing food size. This improvement facilitates the transition between global exploration and local exploitation phases. During the global exploration phase, two distinct walking mechanisms are adopted based on the position of followers, enhancing the algorithm's ability to escape local optima and avoiding premature convergence. In the local exploitation phase, four different neighborhood mechanisms are employed to enhance the optimization capability of the algorithm.

II. CRAYFISH OPTIMIZATION ALGORITHM

The COA simulates the foraging, thermoregulating, and competitive behaviors of crayfish in different scenarios by constructing a mathematical model. This algorithm consists of two phases: the thermoregulation phase and the foraging phase. Changes in temperature affect the behavior of crayfish, causing them to enter different phases. Temperature is defined by Formula 1. When the temperature exceeds 30°C, crayfish will choose a cool place to thermoregulate. At appropriate temperatures, crayfish will engage in foraging behavior. Additionally, the amount of food intake for crayfish is influenced by temperature. The optimal feeding range for crayfish is between 20°C and 30°C. Consequently, the feeding amount of crayfish can be approximated as a normal distribution. Therefore, the temperature range for COA is from 20°C to 35°C, and the mathematical model is as follows:

$$temp = rand \times 15 + 20 \tag{1}$$

Where temp represents the current environmental temperature, and rand is a random number between 0 and 1.

$$p = C_1 \times \left(\frac{1}{\sqrt{2 \times \pi} \times \delta} \times e^{\left(-\frac{(temp-\mu)^2}{2\delta^2} \right)} \right) \tag{2}$$

Here, p is the food intake amount, $C_1 = 0.2$, $\mu = 25$, and $\delta = 3$.

2.1 Thermoregulation phase:

When the temperature exceeds 30°C, the temperature is too high. At this point, crayfish will choose to enter a burrow to thermoregulate. Rapidly seeking out a burrow is a random process. When $rand < 0.5$, it indicates that no other crayfish are competing for the burrow, and the crayfish will directly enter the burrow to cool off. When $rand \geq 0.5$, it signifies that other

crayfish are also interested in this burrow. In this case, they will compete for it. Therefore, the burrow is first defined with the following mathematical formula:

$$X_{shade} = \left(X_G + X_L \right) / 2 \tag{3}$$

Where X_{shade} denotes the burrow position, X_G represents the current optimal position, and X_L is the optimal position of the current population.

Entering the Burrow:

$$X_{i,j}^{t+1} = X_{i,j}^{t} + C_2 \times rand \times \left(X_{shade} - X_{i,j}^{t} \right) \tag{4}$$

Where $X_{i,j}^{t+1}$ signifies the j-th dimensional position of the i-th crayfish in the $t+1$-th iteration, and C_2 is a decreasing curve.

$$C_2 = 2 - \left(t / T \right) \tag{5}$$

Where t indicates the current iteration count, and T is the maximum iteration count.

Competing for the Burrow:

$$X_{i,j}^{t+1} = X_{i,j}^{t} - X_{z,j}^{t} + X_{shade} \tag{6}$$

Where z signifies a randomly selected crayfish individual, as indicated by the following equation:

$$z = int\left(rand \times \left(N - 1 \right) \right) + 1 \tag{7}$$

Where int denotes the integer part.

2.2 Foraging phase:

When the temperature is below 30°C, the conditions are suitable for crayfish to eat. During this time, crayfish will move towards the food. When foraging, crayfish will assess the size of the food. If the food is too large, the crayfish will use their claws to tear off pieces of food before eating; if the food is not large, the crayfish will eat directly. First, the position of the food is defined as follows:

$$X_{food} = X_G \tag{8}$$

Where X_{food} represents the position of the food, which is also the current optimal position of the population.

Food Size:

$$Q = C_3 \times rand \times \left(fitness_i / fitness_{food} \right) \tag{9}$$

Where Q is the food size, C_3 is the food factor representing the maximum food size (constant value of 3), $fitness_i$ denotes the fitness value of the i-th crayfish, and $fitness_{food}$ indicates the fitness value of the food.

Large Food:

The crayfish's judgment of food size comes from the size of the largest food item. When $Q > \left(C_3 + 1 \right) / 2$, it indicates that the food is too large. At this point, the crayfish will use its claws to tear the food before eating. The mathematical equation is as follows:

$$X_{food1} = e^{\left(-\frac{1}{Q} \right)} \times X_{food} \tag{10}$$

When the food is torn into smaller pieces, it is put back into the mouth. To simulate the alternating process, a combination of sine and cosine functions is used. Additionally, the amount of food obtained by the crayfish is also related to the food intake, thus the mathematical equation for foraging is:

$$X_{i,j}^{t+1} = X_{i,j}^{t} + X_{food} \times p \times \left(cos\left(2\pi \times rand\right) - sin\left(2\pi \times rand\right) \right) \tag{11}$$

Small Food:

When $Q \le \left(C_3 + 1\right)/2$, the crayfish only needs to move toward the food and eat directly, as expressed in the following equation:

$$X_{i,j}^{t+1} = \left(X_{i,j}^{t} - X_{food} \right) \times p + p \times rand \times X_{i,j}^{t} \tag{12}$$

During the foraging phase, crayfish adopt different feeding methods based on the size of Q.

III. MIXED STRATEGY IMPROVED CRAYFISH OPTIMIZATION ALGORITHM

The COA is a novel and effective optimization algorithm that can be applied to many optimization problems. However, COA faces challenges when dealing with complex optimization issues, such as slow convergence speed and a tendency to get trapped in local optima. To address these shortcomings, this article introduces a mixed strategy to improve COA, particularly for addressing the weaknesses of the COA in solving complex optimization problems.

3.1 Introduction of improved position update function from the sparrow algorithm:

From the crayfish optimization process, it can be seen that during the foraging phase, the historical optimal crayfish leads, and during the thermoregulation phase, there is a 50% chance to approach the optimal values of the current and historical populations. Therefore, during the exploration process, the crayfish population will quickly converge on the position of the optimal crayfish. This can lead to severe population convergence, making it easy to fall into local optimal solutions, hindering the ability to escape these local optima. Thus, this paper introduces and improves the position update operator of the entrants from the Sparrow Algorithm, sorting the population and selecting the less fit crayfish for disturbance, which enhances randomness and increases the search range, thus increasing the likelihood of escaping local optima and enhancing the global optimization ability of the algorithm. The improved position update function from the Sparrow Algorithm is as follows:

$$w_i = \frac{ln\left(N + 0.5\right) - ln\left(i\right)}{\sum_{j=1}^{N}\left(ln\left(N + 0.5\right) - ln\left(j\right)\right)} \tag{13}$$

Where w_i is the weight coefficient of the i-th ranked crayfish, and N is the population size.

$$X_i^{t+1} = \begin{cases} rand\left(N\left(0{,}5 + 10 \times \frac{i}{N} \times \sqrt{\frac{t}{T}} \right) \right) \times e^{\left(\frac{X_{worst} - X_i^t}{i^2} \right)}, & i > \frac{5}{6}N \\ X_{best}^{t} + \left| w_i \times X_i^t - w_1 \times X_{best}^{t} \right| / \left(w_i + \right) w_1 \times A^{+}, & \frac{2}{3}N < i \le \frac{5}{6}N \end{cases} \tag{14}$$

Where $rand\left(\bullet\right)$ represents the random number generated from the probability density or distribution, X_{worst} indicates the worst individual in the current population, and X_{best}^{t} denotes the optimal position achieved so far. A is a one-dimensional multi-element random matrix with elements of either 1 or -1, and $A^{+} = A^{T}\left(AA^{T}\right)^{-1}$.

3.2 Introduction of improved spiral update position function from the whale optimization algorithm:

During the thermoregulation phase of the crayfish, when the temperature exceeds 30°C, they will either enter a burrow or compete for a burrow. In the original algorithm, only a random selection of a crayfish was used to approach during this

competition, which increased the algorithm's randomness but decreased its convergence. Therefore, the improved spiral update position function from the Whale Optimization Algorithm is introduced as follows:

$$X_i^{t+1} = \left(1 - \left(\frac{t}{T}\right)^2\right) \times \left|X_{best}^t - X_i^t\right| \times e^l \times cos\left(2\pi \times l\right) + X_{best}^t \tag{15}$$

$$l = \left(-2 - \frac{t}{T}\right) \times rand + 1 \tag{16}$$

3.3 Change in the criteria and method for judging food size:

In the original algorithm, crayfish exhibit two behaviors based on food size when foraging, but the criteria for determining food size were too random, causing the algorithm's convergence speed to slow down. Thus, changing the food size judgment criteria is crucial. This paper introduces normalization to alter the food size evaluation criteria as follows:

$$IQ_i^t = \left(fitness_i^t - fitness_{best}^t\right) \Big/ \left(fitness_{worst}^t - fitness_{best}^t + 10^{-300}\right) \tag{17}$$

Where IQ_i^t represents the food size judgment factor, and $fitness_{worst}^t$ denotes the fitness value of the least fit crayfish at iteration t.

3.4 Introduction of the golden ratio coefficient:

In the original algorithm, when crayfish forage for large food items, a temperature-controlled normal distribution was introduced; however, the randomness introduced was insufficient, often leading to small update steps and poor convergence speed. Therefore, the Golden Ratio coefficient is introduced to enhance randomness and increase step length as follows:

$$x_{1,1}^1 = a_1^1 + \left(1 - \frac{\sqrt{5}-1}{2}\right) \times \left(b_1^1 - a_1^1\right) \tag{18}$$

Where $x_{1,1}^1$ represents the Golden Ratio coefficient 1 after its first iteration change, with $a_1^1 = -\pi$ and $b_1^1 = \pi$.

$$x_{1,i+1}^t = \begin{cases} a_i^t + \left(1 - \frac{\sqrt{5}-1}{2}\right) \times \left(b_{i+1}^t - a_i^t\right), \ if \ \ fitness_i^t < fitness_{best}^t \\ x_{2,i}^t, \ if \ \ fitness_i^t \geq fitness_{best}^t \\ a_{i+1}^t + \left(1 - \frac{\sqrt{5}-1}{2}\right) \times \left(b_{i+1}^t - a_{i+1}^t\right), \ if \ \ x_{1,i}^t = x_{2,i}^t \end{cases} \tag{19}$$

Where $x_{1,i+1}^t$ represents the coefficient of the Golden Ratio coefficient 1 after the $i+1$-th change in the t-th iteration, $x_{2,i}^t$ represents the coefficient of the Golden Ratio coefficient 2 after the i-th change in the t-th iteration, a_{i+1}^t represents the iteration change constant 1, and b_{i+1}^t represents the iteration change constant 2, as follows.

$$a_{i+1}^t = \begin{cases} x_{1,i}^t, \ if \ \ fitness_i^t \geq fitness_{best}^t \\ -\pi \times rand, \ if \ \ x_{1,i}^t = x_{2,i}^t \end{cases} \tag{20}$$

$$b_{i+1}^t = \begin{cases} x_{2,i}^t, \ if \ \ fitness_i^t < fitness_{best}^t \\ -\pi \times rand, \ if \ \ x_{1,i}^t = x_{2,i}^t \end{cases} \tag{21}$$

$$x_{2,1}^{1} = a_1^1 + \left(\frac{\sqrt{5}-1}{2}\right) \times \left(b_1^1 - a_1^1\right) \tag{22}$$

Where $x_{2,1}^{1}$ represents the coefficient of the Golden Ratio coefficient 2 after the first change in the first iteration.

$$x_{2,i+1}^{t} = \begin{cases} x_{1,i}^{t}, \ if \ \ fitness_i^t < fitness_{best}^t \\ a_{i+1}^t + \left(\frac{\sqrt{5}-1}{2}\right) \times \left(b_i^t - a_{i+1}^t\right), \ if \ \ fitness_i^t \geq fitness_{best}^t \\ a_{i+1}^t + \left(\frac{\sqrt{5}-1}{2}\right) \times \left(b_{i+1}^t - a_{i+1}^t\right), \ if \ \ x_{1,i}^t = x_{2,i}^t \end{cases} \tag{23}$$

Where $x_{2,i+1}^{t}$ represents the coefficient of the Golden Ratio coefficient 2 after the $i+1$-th change in the t-th iteration.

$$x_1^{t+1} = x_{1,N}^t \tag{24}$$

Where $x_1^1 = x_{1,1}^1$, that is, the coefficient of the Golden Ratio coefficient 1 in the first iteration is equal to the coefficient of the Golden Ratio coefficient 1 after the first change in the first iteration. x_1^{t+1} represents the coefficient of the Golden Ratio coefficient 1 in the $t+1$-th iteration, and $x_{1,N}^{t}$ represents the coefficient of the Golden Ratio coefficient 1 after the last change in the t-th iteration.

$$x_2^{t+1} = x_{2,N}^t \tag{25}$$

Where $x_2^1 = x_{2,1}^1$, that is, the coefficient of the Golden Ratio coefficient 2 in the first iteration is equal to the coefficient of the Golden Ratio coefficient 2 after the first change in the first iteration. x_2^{t+1} represents the coefficient of the Golden Ratio coefficient 2 in the $t+1$-th iteration, and $x_{2,N}^{t}$ represents the coefficient of the Golden Ratio coefficient 2 after the last change in the t-th iteration.

$$X_{i,j}^{t+1} = x_{2,i}^t \cdot X_{i,j}^t \tag{26}$$

3.5 Information accumulation function:

In the original algorithm, the update state of the sorted crayfish upon entering the burrow was not considered. An information accumulation function can be introduced to gradually accumulate self-information. On one hand, this can enhance the approach speed of the leading crayfish, while on the other hand, it can enhance the randomness of the trailing crayfish. The information accumulation function is utilized in the foraging phase of the original algorithm to gradually strengthen self-information attributes, as follows:

$$cos\left(\frac{\pi}{2} \times \left(1 - \left(\frac{3(i-1)}{2N}\right)\right)\right) \tag{27}$$

Application during the cooling phase of entering the burrow:

$$X_{i,j}^{t+1} = cos\left(\frac{\pi}{2} \times \left(1 - \left(\frac{3(i-1)}{2N}\right)\right)\right) \times \left(X_{i,j}^t + C_2 \times rand \times \left(X_{shade} - X_{i,j}^t\right)\right) \tag{28}$$

3.6 Icoa algorithm process:

The algorithm process is as follows:

Step 1: Input: Population size N, initial iteration $t=1$, maximum iteration count T, initial Golden Ratio coefficients 1 and 2, objective function, search space L_b, L_u.

Step 2: Randomly generate the initial population N_i, where $i=1,2,3,\ldots\ldots,N$, and calculate the fitness of the population.

Step 3: Sort based on fitness values, record the optimal individual and target value. Split according to the sorted sequence of crayfish, entering the position update phase for joiners or entering various phases of the original algorithm.

Step 4: Cooling phase and competition phase.

1) When $i \le N/3$, the temperature > 30°C, and $rand < 0.5$, ICOA enters the cooling phase. At this point, COA obtains a new position $X_{i,j}^{t+1}$ based on the cave location (X_{shade}) and the crayfish position ($X_{i,j}^{t}$), and then proceeds to Step 7.

2) When $i \le N/3$, temperature > 30°C, and $rand \ge 0.5$, ICOA enters the competition phase. According to the equation, these two crayfish will compete for the burrow, updating the position X_i^{t+1} based on the optimal position (X_{best}^{t}) using a spiral update. Then, proceed to Step 7.

Step 5: Foraging phase.

1) When $i \le N/3$ and temperature < 30°C, ICOA enters the foraging phase, defining food intake p, food size Q, and food judgment factor IQ.

2) If $IQ > 0.2$, then the food is ground before eating, and continue to Step 7.

Step 6: Joiner position update phase.

1) When $N/3 < i \le 2N/3$, ICOA performs the joiner position update phase, approaching significantly based on the optimal position (X_{best}^{t}), updating to get the new position X_i^{t+1}.

2) When $i > 2N/3$, ICOA performs the joiner position update phase, indicating that the seeker is in a very hungry state, randomly perturbing based on the worst position, and updating to get the new position X_i^{t+1}.

Step 7: Evaluate whether to stop the current generation cycle based on the population and determine whether to exit the cycle. If not, return to Step 3. Otherwise, the algorithm iteration ends, outputting the global optimal value result and the optimal path.

The specific flowchart is as follows, where the red dashed boxes indicate newly added modules, the red formulas represent new formulas, the orange formulas indicate changed original formulas, the green formulas represent additional operators based on the original formulas, and the black formulas indicate formulas that have not been changed.

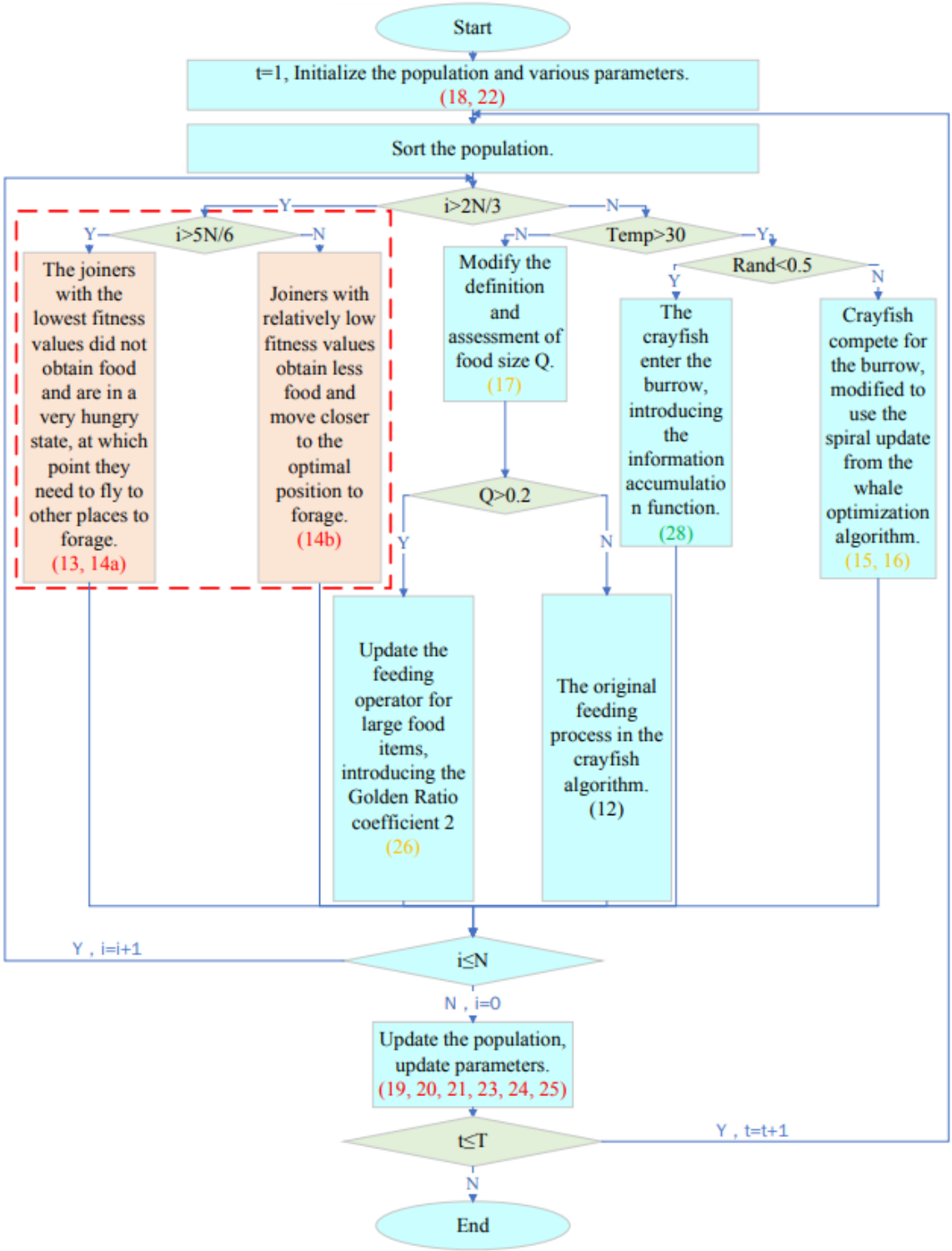

FIGURE 1: ICOA Algorithm Flowchart

IV. SIMULATION EXPERIMENTS AND RESULT ANALYSIS

4.1 Test functions and initialization parameters:

To verify the superiority of the ICOA algorithm compared to other optimization algorithms, this study selects 12 standard test functions that are widely researched to study ICOA. Among these, F1, F2, F3, F4, F6, F7, and F10 are unimodal functions with a single global optimal solution, used to validate the algorithm's local search capability. F5, F8, F9, and F11 are multimodal functions, mainly used to test the algorithm's ability to escape local optima. F12 is a composite function that can be used to test

the algorithm's potential to solve complex optimization problems in the real world. Table 1 presents the functions and their global optima. The results show that ICOA has a significant advantage compared to existing meta-heuristic algorithms and demonstrates good optimization effects and convergence performance. This study uses 12 standard test functions to validate the optimization capabilities of ICOA. This section can be divided into two parts. The first part presents the experimental results and analysis of the 12 standard reference functions. The second part involves comparisons with various classic algorithms. This study compares ICOA with nine popular and modern algorithms: Artificial Bee Colony (ABC), Butterfly Optimization Algorithm (BOA), Grasshopper Optimization Algorithm (GOA), Golden Sine Algorithm (GSA), Moth Flame Optimization Algorithm (MFO), Slime Mold Algorithm (SMA), Teaching-Learning-Based Optimization (TLBO), Whale Optimization Algorithm (WOA), and Crayfish Optimization Algorithm (COA). These algorithms have received considerable attention in swarm intelligence optimization, showing good performance and representativeness. Compared to these algorithms, ICOA can demonstrate its superiority.

This study validates the optimization performance of ICOA using the 12 standard test functions and conducts comparative experiments with nine algorithms. The expressions of the 12 standard test functions can be found in Table 2. The 3D view is shown in Fig 1. The distribution of ICOA across the 12 standard test functions is illustrated in Fig. 2.

TABLE 1
12 STANDARD TEST FUNCTIONS

Function formulation	Dim	Search range	$f_{\min}$
$f_1(x)=\sum_{i=1}^{D}x_i^2$	30	$[-100,100]^D$	0
$f_2(x)=\sum_{i=1}^{D}\lvert x_i\rvert+\prod_{i=1}^{D}\lvert x_i\rvert$	30	$[-10,10]^D$	0
$f_3(x)=\sum_{i=1}^{D}\left(\sum_{j=1}^{i}x_j\right)^2$	30	$[-100,100]^D$	0
$f_4(x)=max_i\left(\lvert x_i\rvert,1\le i\le D\right)$	30	$[-100,100]^D$	0
$f_5(x)=\sum_{i=1}^{D}\left(\lfloor x_i+0.5\rfloor\right)^2$	30	$[-100,100]^D$	0
$f_6(x)=\sum_{i=1}^{D}ix_i^4+random[0,1)$	30	$[-1.28,1.28]^D$	0
$f_7(x)=\sum_{i=1}^{D-1}\left[100\left(x_{i+1}-x_i^2\right)^2+\left(x_i-1\right)^2\right]$	30	$[-10,10]^D$	0
$f_8(x)=\sum_{i=1}^{D}\left(-x_i sin\left(\sqrt{\lvert x_i\rvert}\right)\right)+418.9829\times D$	30	$[-500,500]^D$	0
$f_9(x)=\sum_{i=1}^{D}\left[x_i^2-10cos\left(2\pi x_i\right)+10\right]$	30	$[-5.12,5.12]^D$	0
$f_{10}(x)=-20e^{\left(-0.2\sqrt{\frac{1}{D}\sum_{i=1}^{D}x_i^2}\right)}-e^{\left(\frac{1}{D}\sum_{i=1}^{D}cos(2\pi x_i)\right)}+20+e$	30	$[-32,32]^D$	0
$f_{11}(x)=\frac{1}{4000}\sum_{i=1}^{D}x_i^2-\prod_{i=1}^{D}cos\left(\frac{x_i}{\sqrt{i}}\right)+1$	30	$[-600,600]^D$	0
$f_{12}(x)=\frac{\pi}{D}\left\{10sin^2(\pi y_i)+\sum_{i=1}^{D-1}(y_i-1)^2\left[1+10sin^2(\pi y_{i+1})\right]+(y_D-1)^2\right\}+\sum_{i=1}^{D}u(x_i,10,100,4)$ $y_i=1+\frac{1}{4}(x_i+1),u(x_i,a,k,m)=\begin{cases}k(x_i-a)^m, & x_i>a\\ 0, & -a\le x_i\le a\\ k(-x_i-a)^m, & x_i<-a\end{cases}$	30	$[-50,50]^D$	0

To enhance the fairness of the comparative experiments, this study set the population size to $N = 50$, the maximum number of iterations to $T = 100$, and the dimensionality to $dim = 30$.

4.1.1 Analysis of statistical results for the 12 standard test functions:

Table 2 shows the statistical results obtained after independently running ICOA and the nine comparative algorithms 20 times. The bold parts in the table denote the best results among the 10 algorithms.

TABLE 2
ACCURACY COMPARISON RESULTS OF 10 ALGORITHMS IN 30 DIMENSIONS

Function	Metric	COA	ABC	BOA	GOA	GSA	MFO	SMA	TLBO	WOA	ICOA
$f_1(x)$	Mean	8.777E-151	6021.049	6.60495E-4	241.352	7.849E-58	64926.864	1.049E-54	1246.242	2.463E-1	**0**
	Std	2.633E-150	1399.963	4.525E-05	155.351	2.347E-57	7463.328	3.147E-54	460.114	3.866E-1	**0**
$f_2(x)$	Mean	1.407E-72	46.369	2.623E-2	11.529	4.176E-26	1336026430	5.705E-37	11.788	2.618E-2	**4.627E-284**
	Std	4.220E-72	7.597	7.196E-3	3.182	1.105E-25	2368723731	1.711E-36	2.840	0.016	**0**
$f_3(x)$	Mean	1.160E-167	48427.933	5.964E-4	3552.626	6.295E-52	95461.519	2.969E-33	8907.340	3160.286	**0**
	Std	0	4483.031	4.257E-05	1912.723	1.847E-51	13466.888	8.908E-33	3285.498	3552.179	**0**
$f_4(x)$	Mean	5.287E-85	78.178	1.829E-2	11.366	7.769E-29	85.614	1.476E-26	22.173	7.742	**0**
	Std	1.267E-84	3.960	1.979E-3	2.022	2.307E-28	3.210	4.427E-26	3.882	4.767	**0**
$f_5(x)$	Mean	**0**	6313.100	**0**	210.800	**0**	65373.300	**0**	1600.900	1.100	**0**
	Std	**0**	932.201	**0**	74.917	**0**	6060.215	**0**	694.481	1.578	**0**
$f_6(x)$	Mean	4.767E-4	5.735	**4.642E-4**	0.213	5.843E-4	110.699	8.330E-4	4.137E-1	1.912E-2	5.879E-4
	Std	**3.539E-4**	1.068	4.264E-4	7.636E-2	1.032E-3	25.631	8.754E-4	2.340E-1	8.046E-3	4.678E-4
$f_7(x)$	Mean	28.422	148560.303	28.907	1485.492	4.500E-2	2721211.944	28.695	3319.250	29.235	**2.906E-3**
	Std	3.344E-1	56395.206	2.437E-2	747.658	5.378E-2	386367.247	1.426E-1	2020.238	1.037	**7.017E-3**
$f_8(x)$	Mean	5737.629	8397.505	9224.488	5531.058	**7.904E-1**	8503.890	4660.388	6894.501	5916.009	903.815
	Std	926.593	377.341	319.899	593.694	**4.196E-1**	534.569	422.346	814.259	428.221	1461.886
$f_9(x)$	Mean	**0**	279.883	139.074	149.946	**0**	437.480	**0**	86.645	11.970	**0**
	Std	**0**	16.703	89.153	42.967	**0**	22.486	**0**	14.515	6.181	**0**
$f_{10}(x)$	Mean	**4.441E-16**	16.254	1.305E-2	5.206	**4.441E-16**	20.200	**4.441E-16**	9.594	2.466	**4.441E-16**
	Std	**0**	8.271E-1	1.046E-3	1.080	**0**	1.117E-1	**0**	1.010	5.839	**0**
$f_{11}(x)$	Mean	**0**	51.898	3.801E-3	2.053	**0**	552.423	**0**	12.529	1.965E-1	**0**
	Std	**0**	6.713	6.662E-4	5.224E-1	**0**	40.906	**0**	4.982	1.257E-1	**0**
$f_{12}(x)$	Mean	4.475E-2	135.906	5.418E-1	14.153	2.95597E-4	505.386	1.840E-1	10.471	2.107E-1	**2.150E-06**
	Std	2.287E-2	24.057	9.322E-2	5.230	5.946E-4	52.257	5.151E-2	3.596	1.917E-1	**5.901E-06**

According to the data in Table 2, the ICOA algorithm demonstrates significant superiority in terms of mean values. Specifically, for functions F1 to F5, the ICOA algorithm achieves the theoretical optimal value, while BOA, GSA, SMA, and the original COA only reach the theoretical optimal value for function F5. Additionally, the performance of ICOA in functions F1 to F4 far exceeds that of other algorithms, while the remaining algorithms do not come close to the optimal value for several functions in the above five function tests and even exhibit extremely high values. Not only that, but both COA and ICOA also have

values that are far below those of the other algorithms for these five functions. In functions F7 and F12, the ICOA algorithm also outperforms the other nine algorithms, with results much closer to the optimal solution. It is noteworthy that in the test for function F7, COA fails to escape from local optima, while the improved ICOA algorithm successfully does so, enhancing its optimization results and bringing it closer to the optimal value. In functions F9 to F11, except for ICOA, COA, BOA, GSA, and SMA also reached the theoretical optimal value. However, for function F6, the ICOA algorithm did not outperform the other algorithms, even though its numerical results were very close to those of the best algorithms. In function F8, although ICOA was trapped in a local optimum, it still performed better than the other eight algorithms except for GSA.

In terms of standard deviation, Table 2 shows that the stability of the ICOA algorithm is very reliable. For functions F1 to F5, the ICOA algorithm achieved the theoretical optimal value in all 20 runs, with a standard deviation of 0, whereas BOA, GSA, SMA, and the original COA only exhibited stability in function F5. In functions F1 to F4, these four algorithms displayed some variability, while the other algorithms exhibited significant volatility and performed poorly. Notably, like in terms of mean values, COA and ICOA also have standard deviations that far outperform those of the other algorithms in the aforementioned five functions. In functions F7 and F12, ICOA demonstrated optimal stability in terms of standard deviation in addition to its mean performance. However, the COA algorithm did not show superiority compared to the other algorithms. In functions F9 to F11, COA, BOA, GSA, and SMA also reliably found the optimal solution, with no fluctuations observed over 20 runs, excluding ICOA. In function F6, although the stability of the ICOA algorithm did not reach optimal levels, its standard deviation was not significantly different from the optimal standard deviation, showing only a slight difference. In function F8, although ICOA exhibited strong volatility, this also indicated its ability to escape local optima, making it more likely to find the optimal solution compared to the other eight algorithms, aside from GSA.

In summary, the ICOA algorithm demonstrated clear superiority in terms of mean values, particularly for functions F1 to F5, where its performance far exceeded that of other algorithms, achieving the theoretical optimal value. In functions F7 and F12, the ICOA algorithm also outperformed the other nine algorithms, yielding results that were closer to the optimal solution. Furthermore, regarding standard deviation, the ICOA algorithm exhibited very reliable stability, demonstrating optimal stability in most functions. Although the ICOA algorithm's stability and mean performance did not reach the best levels for certain functions, the difference from the optimal standard deviation was minimal, and it showed the ability to escape local optima in function F8. Therefore, considering the performance of the ICOA algorithm across multiple functions, it is evident that ICOA possesses high optimization performance, demonstrating strong global search ability and good stability.

4.1.2 Analysis of convergence curves for 12 standard test functions:

Fig. 1 presents the convergence curves of the ICOA algorithm and nine other comparative algorithms on 12 standard benchmark functions. By comparing the plots, it can be observed that in functions F1 to F5 and F9 to F11, the ICOA algorithm demonstrates good convergence capability in a 30-dimensional space. Except for function F8, the ICOA algorithm exhibits the fastest convergence speed across the remaining 12 test functions, showcasing excellent convergence ability. Although the convergence speed of the ICOA algorithm in function F8 is slower than that of the GSA algorithm, it still surpasses that of the other eight algorithms. Compared to the original COA algorithm, the ICOA algorithm has made significant improvements in both the optimal values achieved and the speed of convergence. These results indicate that the ICOA algorithm exhibits outstanding convergence capabilities in multidimensional spaces, particularly excelling in high-dimensional scenarios.

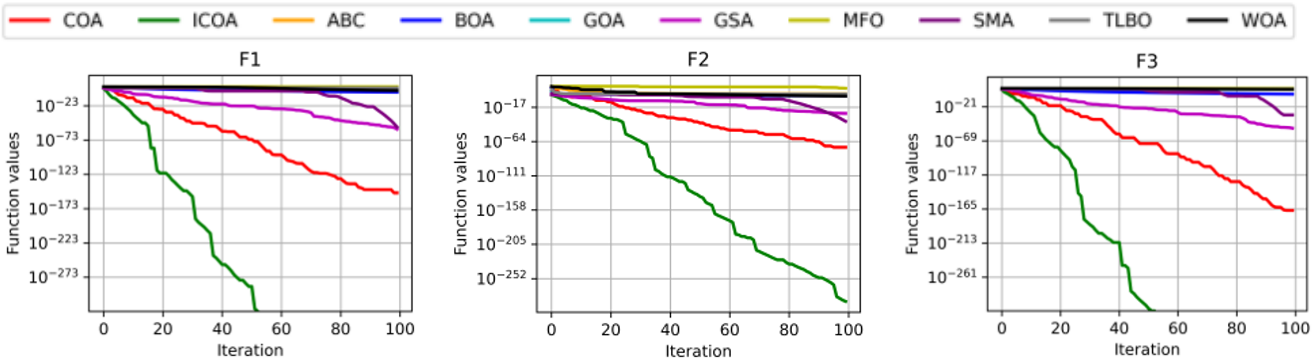

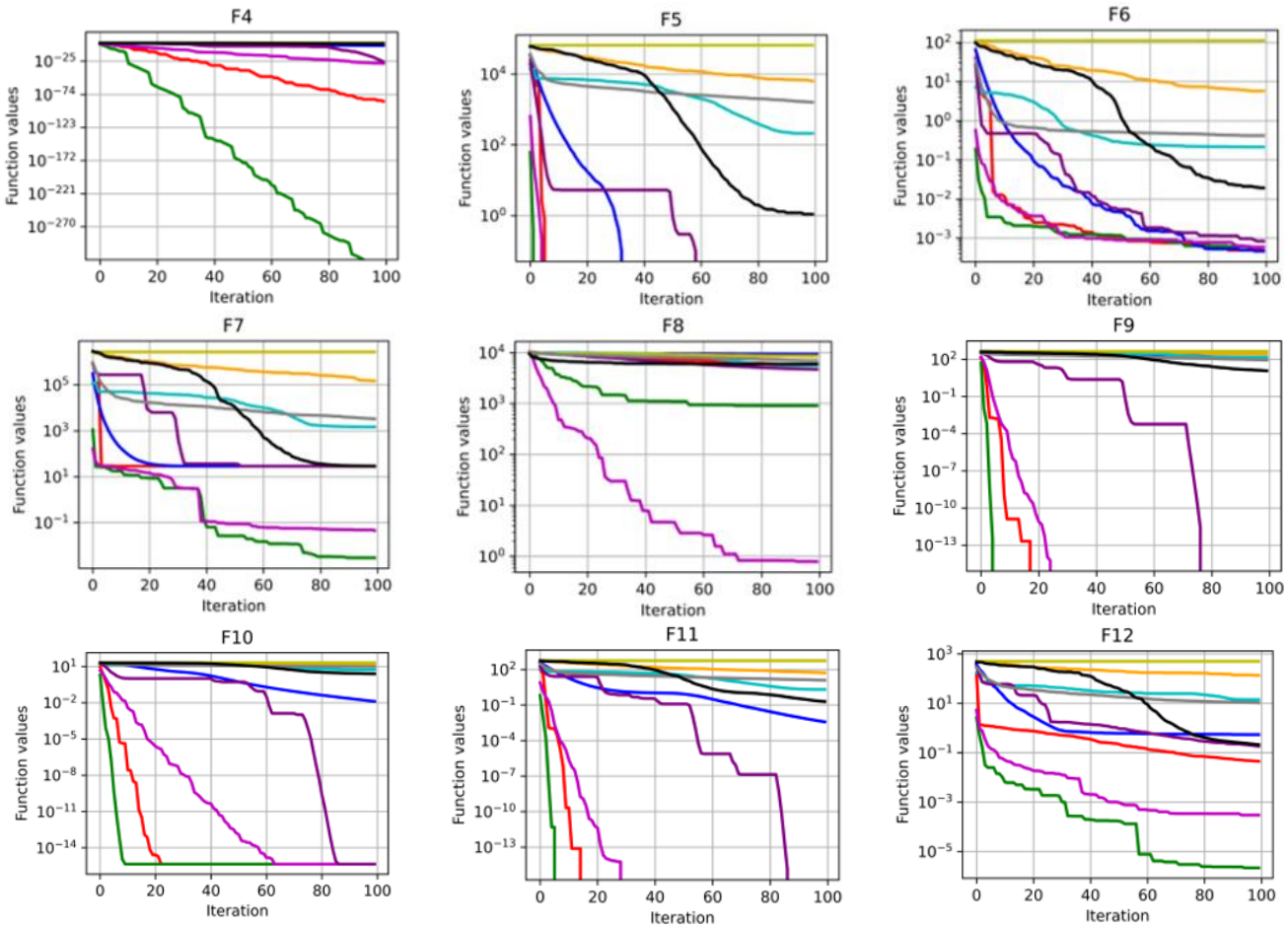

FIGURE 2. Convergence speed of 10 algorithms in 30 dimensions

4.2 Tension/compression spring design problem:

Pressure vessel design is a complex and important engineering field that involves several key issues and challenges. Here are some common research directions:

- **Structural Optimization:** This involves considering the mechanical properties of materials and the geometric shapes of the vessels to reduce weight or costs while meeting strength and stiffness requirements. The goal of structural optimization is to design the most efficient structure that satisfies the functional needs of the vessel while minimizing the use of materials.
- **Material Selection:** Material selection is crucial in pressure vessel design. Researchers need to comprehensively consider factors such as material strength, corrosion resistance, and heat resistance to choose the most suitable materials. The choice of different materials directly impacts the performance and reliability of the vessel.
- **Fatigue Life Prediction:** Given that vessels are subject to cyclic loads during use, fatigue life prediction is an essential research direction in this field. Researchers need to use relevant fatigue analysis methods to consider the fatigue strength of materials and the stress conditions of the vessel to predict its lifespan and take measures to extend its service life.
- **Safety Analysis:** Safety analysis is another critical research direction in pressure vessel design. Researchers must conduct comprehensive analyses and assessments of the vessel's stress state, stress distribution, and deformation to ensure safe operation under various working conditions and to detect and prevent potential safety hazards in a timely manner.
- **Application of Optimization Algorithms:** In recent years, the application of intelligent optimization algorithms in pressure vessel design has received widespread attention. By employing intelligent optimization algorithms such as

genetic algorithms and particle swarm optimization, researchers can more broadly explore design space and find more optimized solutions.

These are some common directions in the research of pressure vessel design, and researchers may choose more specific research topics based on particular needs and challenges. In actual research processes, it is important to integrate knowledge from multiple disciplines, including materials science, structural engineering, mechanics, and thermodynamics, to enhance the performance and reliability of pressure vessels.

The spring design problem addressed in this paper focuses on the tension/compression spring design, aiming to obtain the minimum spring mass under three variables and four constraint conditions. The schematic of the spring is shown in Fig. 3. The variables in the design problem include coil diameter d, mean coil diameter D, and the number of effective coils N. The constraint conditions include minimum deviation (g1), shear stress (g2), impact frequency (g3), and outer diameter limits (g4). By incorporating each variable into the constraint conditions, the minimum spring mass f(x) is derived.

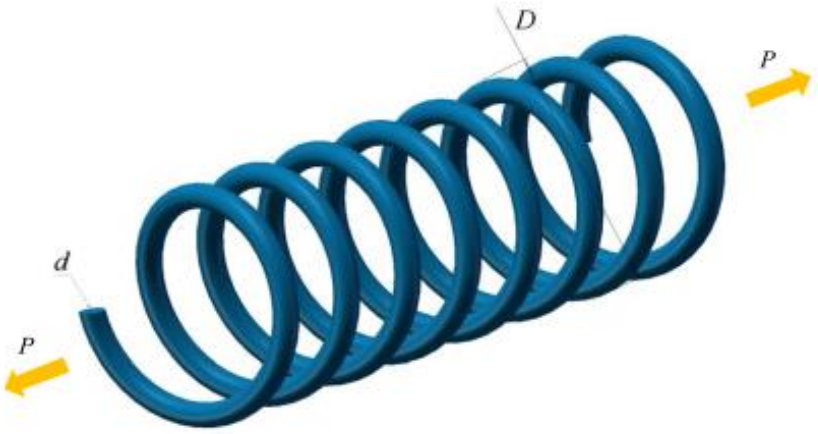

FIGURE 3: Schematic diagram of tension/compression spring design (a)

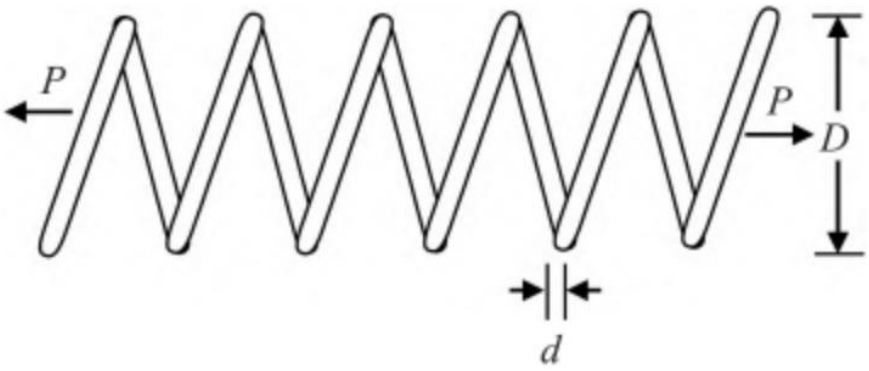

FIGURE 4: Schematic diagram of tension/compression spring design (b)

The mathematical model for this problem is as follows:

$$x=\left[x_1 \;\; x_2 \;\; x_3\right]=\left[d \;\; D \;\; N\right] \tag{29}$$

$$f\left(x\right)=\left(x_3+2\right)\times x_2\times x_1^{\,2} \tag{30}$$

$$g_1\left(x\right)=1-\frac{x_3\times x_2^3}{71785\times x_1^4}\le 0 \tag{31}$$

$$g_2\left(x\right)=\frac{4\times x_2^2-x_1\times x_2}{71785\times x_1^4}+\frac{1}{5108\times x_1^{\,2}}-1\le 0 \tag{32}$$

$$g_3(x) = 1 - \frac{140.45 \times x_1}{x_2^{\,2} \times x_3} \le 0 \tag{33}$$

$$g_4(x) = \frac{x_1 + x_2}{1.5} - 1 \le 0 \tag{34}$$

$$0.05 \le x_1 \le 2,\ 0.25 \le x_2 \le 1.3,\ 2.0 \le x_3 \le 15 \tag{35}$$

Table 3 shows the results of the ICOA and comparative algorithms in the tension/compression spring design problem. From the final data, it is evident that ICOA achieved the optimal value, while other algorithms did not perform as well as ICOA. Fig. 3 and 4 present comparative graphs of the optimal values among various algorithms. They also demonstrate ICOA's convergence speed and optimization capability, confirming that COA effectively addresses the tension/compression spring design problem.

TABLE 3
EXPERIMENTAL RESULTS OF TENSION/COMPRESSION SPRING DESIGN

Optimization Method	d	D	N	Optimal Value
COA	0.06233343	0.655097585	4.335902363	0.01612711
ABC	0.06036433	0.432369438	11.90176535	0.021902094
BOA	1.99279927	0.515235722	5.200026858	1.00E+33
GOA	0.05	0.25	2.35185811	1.00E+33
GSA	0.05	0.25	2	1.00E+33
MFO	0.05	0.315042555	15	0.013389309
SMA	0.05	0.25	2	1.00E+33
TLBO	0.05	0.310725658	15	0.01320584
WOA	0.05	0.31248667	14.73713678	0.01307533
ICOA	**0.05**	**0.3139422**	**14.58918**	**0.013020108**

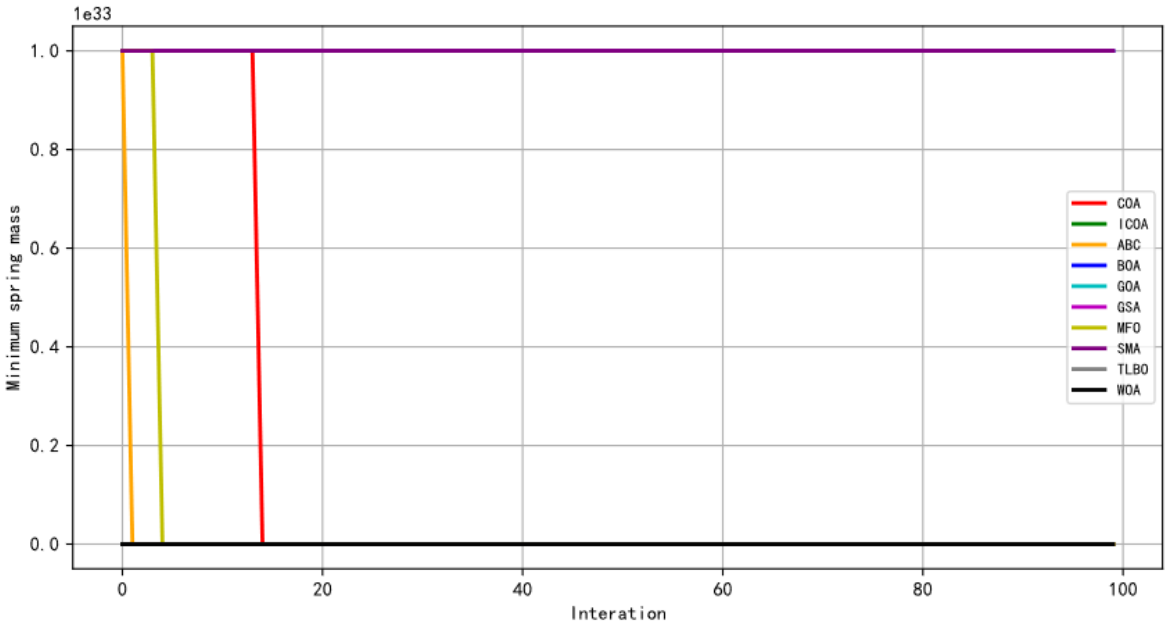

FIGURE 5: Pressure spring design (a)

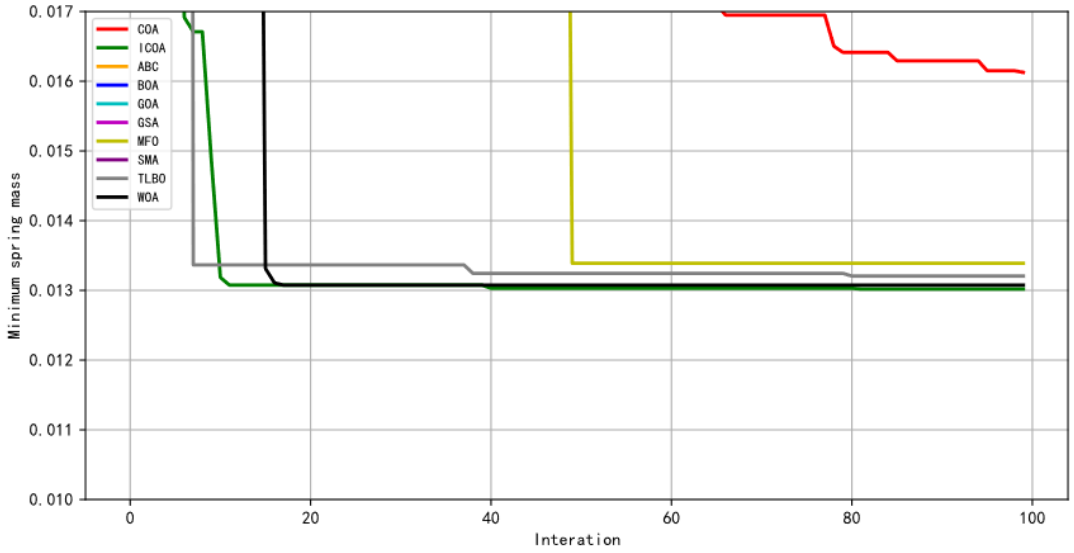

FIGURE 6. Pressure spring design (b)

V. ANALYSIS OF THE CHARACTERISTICS AND OPTIMIZATION ABILITY OF ICOA

5.1 Characteristics of ICOA:

- In ICOA, the algorithm divides the population through sorting and enters different phases based on temperature changes. This method balances the exploration and exploitation capabilities of ICOA more effectively.
- During the updating of participants, the reptiles follow either the optimal or the worst individuals. The update of participants represents the best solution, bringing each individual closer to the optimal or worst values.
- In the cooling phase, the reptiles approach the cave. The cave represents the best solution, enhancing the proximity of each individual to the optimal solution.
- In the competition phase, an improved spiral update position function from the whale optimization algorithm is introduced, enhancing the convergence of the algorithm and speeding up the convergence rate.
- In the foraging phase, the criteria for food size judgment are altered. While maintaining the randomness of the algorithm, the convergence of the algorithm is enhanced. When foraging for larger food sources, the update step size is increased to enhance randomness, and an information accumulation function is introduced to gradually aggregate individual information. This approach increases the speed at which the leading individuals converge and enhances the random abilities of the trailing individuals. The information accumulation function is also introduced when foraging for smaller food sources.

5.2 Optimization ability of ICOA:

Based on the above experimental results and analysis, it can be concluded that ICOA has good optimization performance on 12 standard benchmark functions and 1 engineering problem. In the convergence curves of some test functions, ICOA does not achieve a good purity value at the very beginning of iterations. However, during the iteration process, ICOA can continuously converge to obtain a better optimal solution. This is because the way in which the reptiles approach the cave in the cooling phase demonstrates the algorithm's strong convergence capability. In the participant and foraging phases, the reptiles approach food, improving the algorithm's exploitation ability. Many comparative algorithms tend to get trapped in local optima by the end of iterations, leading to convergence deviation. Although ICOA also experiences local optimum issues in later stages, its exploration and exploitation balance is enhanced by participant updates and temperature adjustments, allowing the algorithm to maintain good convergence capability and achieve satisfactory precision values in subsequent iterations.

VI. CONCLUSION

The improved crayfish optimization algorithm proposed in this paper balances its exploration and exploitation capabilities by filtering participants through sorting and controlling temperature, allowing ICOA to enter different phases. The cooling phase is the exploration phase of ICOA, while the participant and foraging phases represent the development stage of ICOA. The distinct characteristic of this algorithm lies in the exploration and development process based on participant updates and temperature control. During the exploration phase, when a cave is removed, the crayfish enter the cave to escape from high temperatures. The development phase is divided into the participant phase and the foraging phase. In the participant phase, ICOA further splits based on sorting, adopting different cruising strategies. In the foraging phase, ICOA adjusts food size criteria to decide whether to break it up, while foraging is controlled by the amount of food available, allowing for different strategies.

In the experimental section, this paper used 12 standard benchmark functions to verify the optimization effectiveness of ICOA and compared it with 9 different algorithms. The results indicate that ICOA performs well overall, but its exploration capability is somewhat weak, which leads to the algorithm being prone to local optima in later stages. Nevertheless, ICOA maintains good convergence capability in most test functions. After escaping local optima, ICOA can converge rapidly and yield a good solution. The comparative algorithms—ABC, BOA, GOA, GSA, MFO, SMA, TLBO, WOA, and COA—all yield good results in testing functions, but their lack of convergence capability prevents them from escaping local optima in later stages, resulting in lower fitness values. Computational results show that ICOA can achieve better sensitivity values in these engineering problems, indicating its effectiveness in solving practical issues.

This study has validated the effectiveness of ICOA in solving optimization problems using 12 standard benchmark functions and engineering problems. In future work, we will further enhance the exploration capability of ICOA and apply this algorithm to solve practical engineering problems such as three-dimensional path planning for drones, feature selection, image processing, and multi-threshold image segmentation.

REFERENCES

[1] Dantzig G B. Linear programming[J]. Operations research, 2002, 50(1): 42–47.

[2] Chen H, Chen L, Zhang G. Block-structured integer programming: Can we parameterize without the largest coefficient?[J]. Discrete Optimization, 2022, 46: 100743.

[3] Daryalal M, Bodur M, Luedtke J R. Lagrangian dual decision rules for multistage stochastic mixed-integer programming[J]. Operations Research, 2024, 72(2): 717-737.

[4] Gautier A, Granot F. On the equivalence of constrained and unconstrained flows[J]. Discrete applied mathematics, 1994, 55(2): 113-132.

[5] Ezugwu A E, Shukla A K, Nath R, et al. Metaheuristics: a comprehensive overview and classification along with bibliometric analysis[J]. Artificial Intelligence Review, 2021, 54: 4237-4316.

[6] Dréo J. Metaheuristics for hard optimization: methods and case studies[M]. Springer Science & Business Media, 2006.

[7] Holland J H. Adaptation in natural and artificial systems: an introductory analysis with applications to biology, control, and artificial intelligence[M]. MIT press, 1992.

[8] Karaboga D. Artificial bee colony algorithm[J]. scholarpedia, 2010, 5(3): 6915.

[9] Arora S, Singh S. Butterfly optimization algorithm: a novel approach for global optimization[J]. Soft computing, 2019, 23: 715-734.

[10] Meraihi Y, Gabis A B, Mirjalili S, et al. Grasshopper optimization algorithm: theory, variants, and applications[J]. Ieee Access, 2021, 9: 50001-50024.

[11] Tanyildizi E, Demir G. Golden sine algorithm: a novel math-inspired algorithm[J]. Advances in Electrical & Computer Engineering, 2017, 17(2).

[12] Mirjalili S. Moth-flame optimization algorithm: A novel nature-inspired heuristic paradigm[J]. Knowledge-based systems, 2015, 89: 228-249.

[13] Li S, Chen H, Wang M, et al. Slime mould algorithm: A new method for stochastic optimization[J]. Future generation computer systems, 2020, 111: 300-323.

[14] Rao R V, Savsani V J, Vakharia D P. Teaching–learning-based optimization: an optimization method for continuous non-linear large scale problems [J]. Information sciences, 2012, 183(1): 1-15.

[15] Mirjalili S, Lewis A. The whale optimization algorithm[J]. Advances in engineering software, 2016, 95: 51-67.

[16] Jia H, Rao H, Wen C, et al. Crayfish optimization algorithm[J]. Artificial Intelligence Review, 2023, 56(Suppl 2): 1919-1979.

[17] Mzili T, Riffi M E, Mzili I, et al. A novel discrete Rat swarm optimization (DRSO) algorithm for solving the traveling salesman problem[J]. Decision making: applications in management and engineering, 2022, 5(2): 287-299.

[18] Jia H, Sun K, Li Y, et al. Improved marine predators algorithm for feature selection and SVM optimization [J]. KSII Transactions on

Internet and Information Systems (TIIS), 2022, 16(4): 1128-1145.

[19] Jia H, Zhang W, Zheng R, et al. Ensemble mutation slime mould algorithm with restart mechanism for feature selection[J]. International Journal of Intelligent Systems, 2022, 37(3): 2335-2370.

[20] Mzili I, Mzili T, Riffi M E. Efficient routing optimization with discrete penguins search algorithm for MTSP [J]. Decision Making: Applications in Management and Engineering, 2023, 6(1): 730-743.

[21] Liu Q, Li N, Jia H, et al. Modified remora optimization algorithm for global optimization and multilevel thresholding image segmentation[J]. Mathematics, 2022, 10(7): 1014.

[22] Das M, Roy A, Maity S, et al. Solving fuzzy dynamic ship routing and scheduling problem through new genetic algorithm[J]. Decision Making: Applications in Management and Engineering, 2022, 5(2): 329-361.

[23] Qi H, Zhang G, Jia H, et al. A hybrid equilibrium optimizer algorithm for multi-level image segmentation[J]. Math Biosci Eng, 2021, 18(4): 4648-4678.

[24] Wen C, Jia H, Wu D, et al. Modified remora optimization algorithm with multistrategies for global optimization problem[J]. Mathematics, 2022, 10(19): 3604.

[25] Wolpert D H, Macready W G. No free lunch theorems for optimization[J]. IEEE transactions on evolutionary computation, 1997, 1(1): 67-82.

Strength Analysis of an Archimedes Wind Turbine Model Designed for Additive Manufacturing

Ivan Mihálik[1*]; Marián Lázár[2]; Natália Jasminská[3]; Tomáš Brestovič[4]; Peter Čurma[5]; Lukáš Simočko[6]

Department of Energy Engineering, Faculty of Mechanical Engineering, Technical University of Košice, 042 00 Košice, Slovakia
*Corresponding Author

Received: 06 October 2024/ Revised: 14 October 2024/ Accepted: 19 October 2024/ Published: 31-10-2024

Abstract— *The article examines the Archimedes wind turbine model with a diameter of 1,500 mm in terms of the strength of its construction. It describes in detail the material properties of the turbine produced by means of alternative methods, specifically by means of the Selective Laser Sintering additive technology. By combining CFD simulation and strength analysis, the article solves the influence of the pressure force of the wind and the speed of the turbine on the tension and deformations in its construction. The results are compared with commercially available turbines made of composite materials.*

Keywords— Wind Energy, Wind Turbine, Strength Analysis, Computational Fluid Dynamics.

I. INTRODUCTION

Research and development of new special types of wind turbines makes it possible to use the huge potential of wind energy in the world in areas where the application of conventional wind turbines is not suitable. One of the many types of wind turbines is the so-called Archimedes wind turbine, the development of which has been ongoing since the beginning of the 21st century. The design of the turbine minimizes the negative aesthetic impact on the surroundings. At the same time, the essence of the design forces the turbine to rotate automatically in the direction of the wind, which results in less demanding operation. From this point of view, the device is suitable, for example, for use for private purposes in densely populated areas. Therefore, increased safety requirements are placed on its operation, and it is necessary to know the strength limits of the device, so that during its operation there is no damage to it and subsequent damage to health and property.

II. PARAMETERS OF THE INVESTIGATED TURBINE

A 3-bladed Archimedes turbine with a diameter of 1,500 mm was subjected to strength analysis in order to test the mechanical strength of the turbine. A detailed view of the geometry of the individual stages of blades with an inclination of 60/50/65° is shown in Fig. 1:

FIGURE 1: Geometry of the Archimedes turbine model

The material from which the Archimedes turbine is to be made is Nylon PA12 in powder form, while production is being considered through the SLS (Selective Laser Sintering) additive method. It is a 3D printing method that uses a high-powered laser to fuse together small particles of plastic, metal, glass, or ceramic powder into a solid object. Among the various additive manufacturing methods, this is the most suitable method for the production of functional prototypes in terms of their strength. At the same time, compared to other types of 3D printing, this method enables the production of larger parts, moreover, in a shorter period of time. The material properties of Nylon PA12 are listed in Tab. 1:

TABLE 1
PROPERTIES OF NYLON PA12

Density	1,010 $kg \cdot m^{-3}$
Molar mass	226.3 $g \cdot mol^{-1}$
Young's modulus	$1.8 \cdot 10^{9}$ Pa
Poisson's ratio	0.39
Yield strength	$4.8 \cdot 10^{7}$ Pa

When the turbine rotates, two main force components act on it. The first component is the wind force, represented by the pressure gradient on the surface of the turbine. The second component is the centrifugal force, which is a function of the angular velocity and diameter of the turbine. The design maximum of similar turbines made of composite materials applied in practice corresponds to a wind speed of 35 $m \cdot s^{-1}$. This data was used as the starting value of the wind speed together with the turbine speed of 10 $rev \cdot s^{-1}$. The monitored parameters were the tension and deformation of the turbine.

III. PARAMETERS OF STRENGTH ANALYSIS

The analysis also investigated the effect of wind pressure on the overall stress of the turbine. For this reason, two simulations were carried out, the first with the effect of wind and the second with only centrifugal force. The strength analysis was performed in the ANSYS software through the Static structural module. This is a module that works on the basis of numerical simulations using the finite element method. Since the wind pressure gradient also plays role in the strength analysis, it is necessary to link the CFD simulation performed using the "ANSYS CFX" module with the "Static structural" module. The ANSYS CFX module works on the principle of the finite volume method and is a powerful tool designed for simulations of fluid flow and thermal processes.

First, the CFD simulation settings were defined, while the Tetrahedrons method with a basic element size of 24 mm was used to create the network. The tetrahedral structure is suitable because it can define the complex shapes of turbine blades. In places where a steady state of pressures and velocities is expected, such as on the peripheral parts of the air tunnel model, it is advisable to choose a larger element size. Based on knowledge of hydrodynamics, it is necessary to take into account that even during turbulent events, such as when air flows around the turbine, a thin layer of air is created near the surface of the turbine, which has a laminar character. Neglecting the laminar layer would affect the accuracy of the calculation, so it is necessary to modify the network so that the elements in close proximity to the turbine form continuous surrounding layers. Type k-ε was chosen as the turbulence model. The turbine body was assigned a material with material properties defined from Tab. 1. Subsequently, a CFD simulation of air flow with a speed of 35 $m \cdot s^{-1}$ at 10 $rev \cdot s^{-1}$ was started.

After completing the CFD simulation, the parameters of the Static Structural simulation were defined. In the Engineering Data tab, a turbine material with the same properties as in the previous simulation was created. In the Model tab in the Geometry item, all bodies representing air were suppressed. Similar to the previous simulation, the mesh was created using the Tetrahedrons method, while the size of the elements was defined as 12 mm.

Acting forces and boundary conditions were defined in the Static Structural GDS item. By inserting the Rotational velocity function, the angular velocity of the turbine was defined for the Y Component, as the turbine rotates around the Y axis. At 10 $rev \cdot s^{-1}$, its angular velocity is equal to 62.4 $rad \cdot s^{-1}$. The next step is to define the boundary conditions in order to remove the degrees of freedom of the turbine body. The Cylindrical support function was used to define the rotation and then the rotor surfaces were selected, thereby removing four degrees of freedom from the body. The last degree of freedom was removed through the Displacement function, where the Y Component was defined with a value of 0 mm, allowing the body to move in the Y axis by a zero value. For this reason, the turbine can only move by rotating around the Y axis.

The pressure gradient acting on the turbine was subsequently imported from the performed CFD simulation via the Imported load item. In the function Imported pressure, the surfaces of the turbine were set as the geometry, which defined the places of pressure action. As the last step, the total deformation of the body measurements and von-Mises equivalent stress measurements were defined in the Solution item. After finishing the preparation of the simulation model, the strength analysis itself was performed.

IV. RESULTS OF STRENGTH ANALYSIS

The turbine with a diameter of 1,500 mm was subjected to a maximum stress of 341 MPa at a wind speed of 35 $m \cdot s^{-1}$ and a speed of 10 $rev \cdot s^{-1}$. This stress exceeds the yield strength of the selected material seven times, which would cause complete destruction of the turbine at the specified wind parameters. To compare the effect of the pressure caused by the flowing wind, a simulation was performed with the same settings, but without the effect of the imported pressure. The results of both simulations and their comparison are shown in Tab. 2. From the results of the simulations, it is obvious that the stress difference between the two simulations is at a maximum of 1.54 MPa and at an average value of 0.06 MPa. Based on these findings, it can be concluded that the pressure effect of the wind can be neglected even in extreme weather conditions. However, it should be noted that it is possible to neglect only the pressure effect of the wind and not its high speeds, since high wind speeds directly cause the high revolutions of the turbine leading to its destruction.

TABLE 2
STRESS AND DEFORMATION AT A WIND SPEED OF 35 $m \cdot s^{-1}$ AND A TURBINE SPEED OF 10 $rev \cdot s^{-1}$

The effect of imported pressure	Stress (MPa)			Deformation (mm)		
	Min.	Med.	Max.	Min.	Med.	Max.
With pressure load	$4.51 \cdot 10^{-5}$	15.35	341.78	0	313.4	1885.3
Without pressure load	$5.89 \cdot 10^{-5}$	15.29	340.24	0	312.11	1878.5

Since the turbine was destroyed at a speed of 10 $m \cdot s^{-1}$, it was necessary to determine the maximum speed at which the stress on the turbine would not exceed the yield strength value. Stresses and deformations were analyzed by gradually adjusting the speed, and based on the previous simulations, the pressure effect of the wind was neglected. Fig. 2 shows the course of stress and deformation at different turbine speeds. At a value of 4 $rev \cdot s^{-1}$, the maximum stress was 53.6 MPa, which still exceeds the yield strength. When the speed was subsequently reduced to a value of 3.5 $rev \cdot s^{-1}$, the maximum stress was reduced to a value of 41 MPa, which is the permissible value of the turbine load. When the speed was reduced to 3 $rev \cdot s^{-1}$, the maximum stress was equal to 30.2 MPa with a maximum deformation of 227 mm at the tip of the blade. From the course of the graph, an exponential growth of both stress and deformation is visible with increasing revolutions.

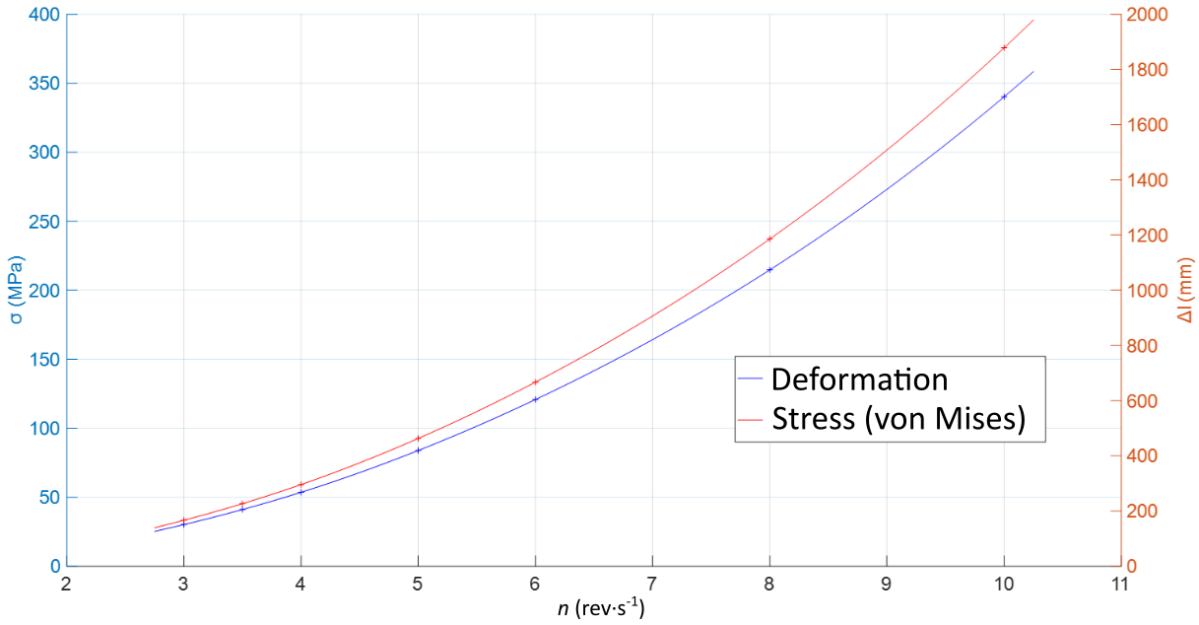

FIGURE 2: Dependence of stress and deformation on turbine speed

From the stress and deformation gradients, it is obvious that the rear part of the turbine is the most affected. The maximum stress occurs at the joint of the blades and the rotor, despite the roundness of the edge of the blades. When the yield point is exceeded, a crack will appear just at the back of the connection between the blade and the rotor. The first stage of the turbine blade is the most affected in terms of deformation. This is because the second and third stages are fixed to the shaft, while the first stage is not fixed by anything on the trailing edge of the blade. Areas of maximum stress are indicated by arrows in Fig. 3.

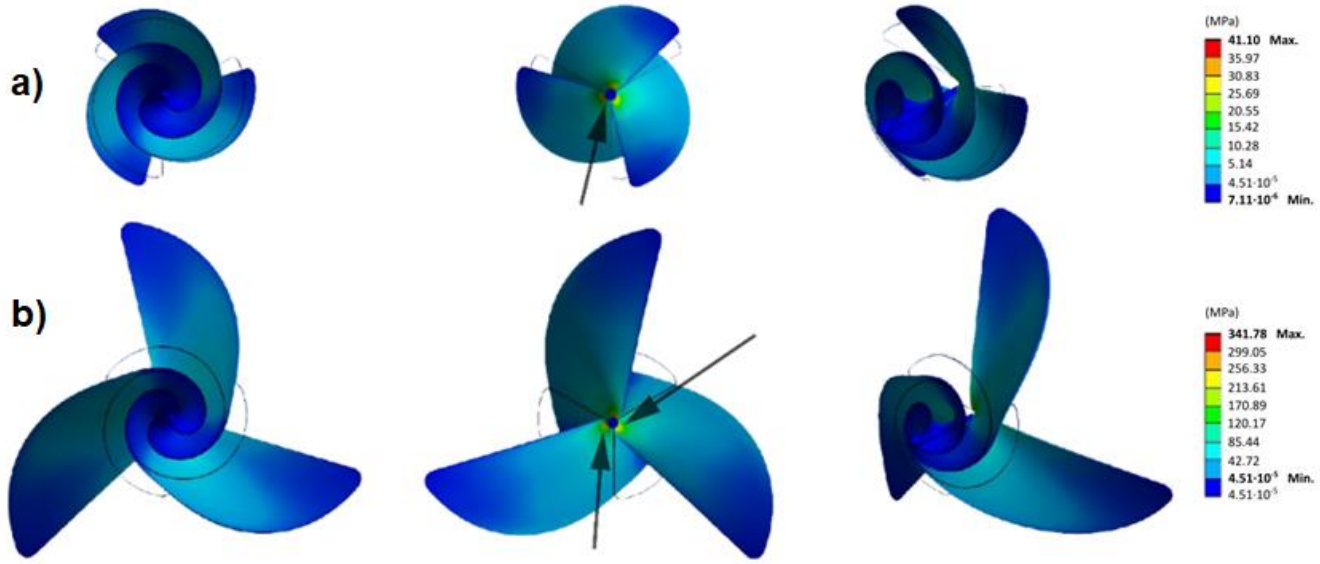

FIGURE 3: Von Mises stress: a) at 3.5 rev·s^{-1}; b) at 10 rev·s^{-1}

The deformation can be clearly observed by looking at Fig. 4, on which the original dimensions of the turbine are marked with black outlines. While the deformation of the turbine at 3.5 rev·s^{-1} is still acceptable due to the mechanical properties of the turbine, the deformation shown in Fig. 4b) is unattainable in practice due to several times exceeding the yield point at 10 rev·s^{-1}, since the turbine will be destroyed before such a level of deformation is reached.

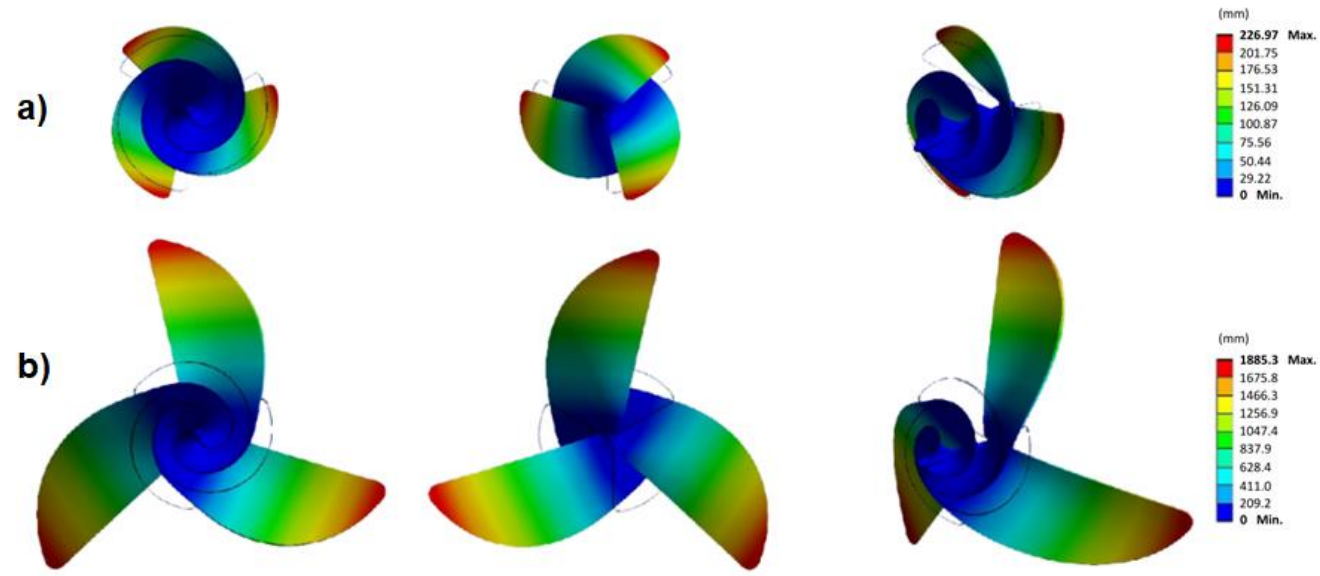

FIGURE 4: Turbine deformation: a) at 3.5 rev·s^{-1}; b) at 10 rev·s^{-1}

There are two options for increasing the mechanical strength of the turbine without significantly affecting its aerodynamics. The first solution is to use stronger and more rigid materials, ideally with a density similar to that of nylon PA12. The second solution is the use of reinforcements in the form of steel rods that connect the individual blades, which ensures higher turbine rigidity and lower applied stress.

V. CONCLUSION

Considering the development of events in the world in recent years, the Archimedes wind turbine can serve as one of the ways of diversifying energy sources for small companies and households, which could contribute to increasing their independence and stability. The production of electricity through wind power itself does not produce waste, does not pollute the air and does not have a negative impact on people's health. These are the most important reasons for the development of innovative equipment in the field of wind energy use. Commercially used Archimedes wind turbines are usually made from a single piece of composite material consisting of plastic and fiberglass. An alternative is the production of turbines through additive methods, which, however, results in a difference in the strength properties of the turbine. The maximum revolutions at which the examined turbine with a diameter of 1,500 mm, made by the additive method from the material Nylon PA12, is able to work without damage is 3.5 $rev \cdot s^{-1}$, at which it reaches a maximum stress of 41 MPa. Improving the durability of the turbine can be achieved without changing the material, for example by applying reinforcements in the space between the blades.

ACKNOWLEDGEMENTS

This paper was written with financial support from the VEGA granting agency within the projects no. 1/0224/23 and no. 1/0532/22, and from the KEGA granting agency within the project no. 012TUKE-4/2022.

REFERENCES

[1] H.S.A. Hameed et al., “Shape optimization of a shrouded Archimedean-spiral type wind turbine for small-scale applications,” in Energy, January 2023, Vol. 263, Part B, 125809.

[2] K. CH. Kim et al., “Experimental and Numerical Study of the Aerodynamic Characteristics of an Archimedes Spiral Wind Turbine Blade,” in Energies, November 2014, Vol. 7, No. 12, pp. 7893-7914.

[3] J. K. Kaldellis, D. P. Zafikaris, “Trends, Prospects, and R&D Directions in Wind Turbine Technology,” in Comprehensive Renewable Energy, 2012, Vol. 2, pp. 671-724.

[4] M. A. A. Nawar et al., “Experimental and numerical investigations of the blade design effect on Archimedes Spiral Wind Turbine performance,” in Energy, May 2021, Vol. 223, 120051.

[5] Y. Patil, “Design, Fabrication and Analysis of Fibonacci Spiral Horizontal Axis Wind Turbine,” in International Journal of Aerospace and Mechanical Engineering, January 2018, Vol. 5, No. 1.

[6] T. Brestovič, N. Jasminská, Numerické metódy a modelovanie v energetike. 1st edition, 2015, Košice: Technical University of Košice, Faculty of Mechanical Engineering, 117 p., ISBN 978–80–553–0223–2.

[7] A. V. da Rosa, J. C. Ordóñez, “Chapter 15 - Wind Energy,“ in Fundamentals of Renewable Energy Processes, 4th edition, Academic Press, 2022, p. 721-794.

Research into the Possibilities of Burning Hydrogen and Fossil Fuel with the Aim of Reducing its Carbon Footprint

Peter Milenovský[1*], Natália Jasminská[2], Marián Lazár[3], Tomáš Brestovič[4], Peter Čurma[5]

Department of Energy Engineering, Faculty of Mechanical Engineering, Technical University of Košice, Slovakia
*Corresponding Author

Received: 08 October 2024/ Revised: 16 October 2024/ Accepted: 24 October 2024/ Published: 31-10-2024

***Abstract*—** *Requirements for increasing the environmental friendliness of electricity and heat production to reduce the emission footprint are increasing the demands on the used fuels. For the replacement of conventional fuels in the process of combined production of electricity and heat, it is possible to use synthetic gases, which are created during processes of thermal recovery of biomass and waste. The presented article discusses the possibilities of using synthesis gas obtained by thermal recovery of waste in a plasma reactor in cogeneration units. For the experiment, different ratios of mixtures of natural gas and synthesis gas were used to reduce the consumption of fossil fuel without significantly reducing the performance of the cogeneration unit. The primary combustibles in the synthesis gas were hydrogen and carbon monoxide, the calorific value of which differs from that of methane, causing changes in fuel consumption to maintain the required unit performance. For the full possibility of using synthesis gas as a replacement in cogeneration units, further research is necessary both in the field of its use in combustion engines and in the field of its acquisition and primary purification.*

Keywords*— *Hydrogen, Cogeneration Unit, Syngas, Renewable Fuels.

I. INTRODUCTION

Between 2010 and 2020, it is possible to observe a total decrease in the production of greenhouse gases in the form of CO_2. This decrease is caused by many factors, including the global COVID-19 pandemic, which caused a significant slowdown in the economy in 2020, and the associated lower amount of CO_2 emissions produced. In addition to this sudden drop in production, the EU's commitment to meeting the requirements of the Kyoto Protocol and the provisions on the decarbonization of Europe by 2050 has a significant impact on reducing CO_2 emissions.

The decrease in the amount of CO_2 produced in Slovakia between 2010 and 2020 was around 19%, while to meet the EU requirements for the overall reduction of CO_2 production, an increase in efforts and thus more significant changes in the field of industry and transport are necessary. The total amount of CO_2 produced by transport in Slovakia in 2020, including both passenger and freight transport, amounted to 31.163 mil. tons. According to the data of the Statistical Office of the Slovak Republic, the share of CO_2 production by transport in the total amount of CO_2 produced is increasing, which increased from 6.08% to 12.52% between 2010 and 2020 [1]. Due to the significant increase in the share of transport in the total production of CO_2, it is necessary to focus on reducing CO_2 not only in industry, but also in transport. Increasing the use of hydrogen in transport has a significant impact on the elimination of CO_2 production and increases the possibilities of meeting the EU's decarbonisation goals.

Hydrogen transport, as well as alternative gaseous mixed fuels containing a significant proportion of hydrogen, are based on the idea of using hydrogen as a basic energy carrier. Vehicles that use hydrogen fuel for their propulsion are generally referred to as hydrogen vehicles. Hydrogen vehicles are divided into two basic categories according to the method of converting the chemical energy of hydrogen into mechanical energy. Hydrogen fuel cell vehicles (HFCV - Hydrogen Fuel Cell Vehicle) belong to the first and currently the most widespread category of hydrogen vehicles. The second category consists of vehicles with a hydrogen combustion engine (HICEV - Hydrogen Internal Combustion Engine Vehicle), whose representation on the automobile market is currently almost zero. The process of burning hydrogen is like that of other high-temperature fuels, such as petrol, diesel or natural gas. However, the achieved efficiency of a hydrogen-burning engine is fundamentally lower compared to a fuel cell. However, the investment costs of a hydrogen combustion engine are also lower compared to a fuel

cell. At the same time, it is possible to use already existing equipment, which, after transformation, enables adaptation to the new ecological fuel.

Assuming the combustion of only pure hydrogen in the exhaust gases, there are no carbon-based pollutants, such as carbon monoxide CO or carbon dioxide CO_2, just like when using a fuel cell. Due to the combustion of hydrogen in an atmosphere containing nitrogen and oxygen, however, undesirable nitrogen oxides, also known as NO_X, can be produced during the combustion process. Despite the shortcoming, internal combustion engines burning gaseous fuel based on hydrogen can be one alternative facilitating the transition of industry and transport to 100% clean and green technologies.

In 2011, a team led by Iwasaki Hideyuki from “Tokyo City Univ.” published the results of implementing direct combustion hydrogen propulsion in turbocharged engines into two city vehicles, namely a small city bus and a small city van. The result of the implementation were two functional prototypes of vehicles with direct hydrogen combustion, while each of them used a partially different approach to the given issue. Both vehicles were equipped with the N04-H2 combustion engine, with one of the engines using TCI (transistor coil ignition) technology, while the other engine used CDI (Capacitor discharge ignition) technology. In both cases, the fuel was hydrogen compressed at high pressure. Research on real vehicles has proven the suitability of using hydrogen in direct combustion, with the addition that many sub-problems in the process of direct hydrogen combustion still need to be solved [2].

Following the research carried out at “Tokyo City Univ.” It is also worth mentioning the work of a team led by S. Natarajan from the “Indian Institute of technology – Delhi” created 15 three-wheeled hydrogen vehicles of the “Rickshaw” type by Mahindra, which were equipped with a single-cylinder four-stroke engine with a volume of 395 cm^3. As a result, it was found that at full load there was a decrease in performance compared to the gasoline variant by about 25%, while this decrease was caused by a depleted fuel mixture. During the test run, small shares of CO and CO_2 were recorded at the output due to the partial combustion of oil by the engine, and at the same time negligible shares of NO_X compared to conventional combustion engines. Experimental measurements also proved that the given types of internal combustion engines can be rebuilt to burn hydrogen without major interventions in the overall structure of the engine and without significant performance losses [3].

In addition to the use of diesel and possibly gasoline as a moderator of hydrogen combustion in direct combustion engines, the use of CNG and compressed natural gas can also be considered. These are combustion engines marked HCNG. In this case, there is a need to address the excessive amount of NOx generated due to high operating temperatures in the combustion chamber, as reported by R.K. Mehra and the team from "State Key Laboratory of Automobile Safety and Energy, Tsinghua University, Beijing 100084, People's Republic of China" [4]. The laminar burning speed of hydrogen/air is about six times that of gasoline/air. Due to this higher burning rate, the actual indicator diagram has moved closer to the ideal, resulting in a higher thermal efficiency of the engine [5]. The synthesis of air and a small amount of hydrogen gas produced a combustible mixture that can be burned in a conventional spark-ignition engine below the limit of a lean gasoline/air mixture. Combustion of gasoline/air and hydrogen in a very lean mixture provides a lower flame temperature, resulting in less heat transfer, higher thermal efficiency and reduced NOx emissions [6].

In view of the definitive approval of the ban on the sale of new vehicles with a conventional drive in the territory of the EU states from 2035 and the EU's goals in the field of decarbonization of industry, it is necessary to intensify research in the search for ecological and at the same time effective low-emission fuel alternatives and think rationally about the possibility of transforming already existing technologies into devices using hydrogen as fuel. The submitted contribution analyses the possibility of energy recovery of synthesis gas produced in the process of high-temperature gasification of waste using a combustion engine recovering a mixture of natural gas and synthesis gas.

II. CO-COMBUSTION OF SYNTHESIS GAS AND NATURAL GAS IN A SPARK-IGNITION ENGINE

Synthesis gas produced in the process of high-temperature gasification of waste in a plasma reactor can be considered as an alternative secondary fuel, which is created e.g. in the process of energy recovery of unusable and otherwise non-recyclable waste. With a significant representation of the plastic fraction of the input mixture of wastes entering the plasma gasification process, the calorific value of syngas is at the level of 12-15 $MJ \cdot m^3$ of the gas mixture, while hydrogen can have up to 50 vol. % representation in syngas. Based on the results of high-temperature gasification of various types of waste, the artificially mixed mixture of synthesis gas, which was used in the experiments, consisted of the four most dominant gas elements (CH_4, CO, H_2, N_2) represented in real samples of synthesis gas. Their percentage representation in the mixed gas mixture is adapted to the composition of the collected samples of syngas generated from RDF and municipal waste and to the technological and safety requirements associated with the storage of explosive gas mixtures in pressure vessels. The percentage of components

represented in the mixed mixture of gases corresponds to the values of 45 vol. % H_2, 40 vol. % CO, 5 vol. % CH_4 and 10 vol. % N_2. The mixture of syngas and natural gas prepared in this way is then, after passing through the mixing chamber, energy-enhanced in the cogeneration unit, the drive unit of which is a converted four-cylinder spark-ignition combustion engine with a working volume of 1584 cm3. Engine power at 5,000 rpm is 55 kW. Its compression ratio is 8,8:1, the number of valves per cylinder - 2, while the original fuel was 95 octane gasoline. The original system used to prepare the fuel mixture for a spark-ignition combustion engine from easily vaporizable liquid fuels (carburettor) was modified to a system enabling the combustion of gaseous fuel mixtures (by installing a gas fuel mixer). The mechanical power of the four-cylinder spark-ignition combustion engine to the asynchronous generator (TGL 11856/01, type KHR 132 M4) is transmitted by means of a shaft. An asynchronous generator, used mainly in cogeneration units with a small power (up to 100 kW), works in parallel with the superior electrical system. The start of the cogeneration unit is provided by the generator by starting the combustion engine in motor mode. When the nominal speed is reached, the combustion engine takes over the load and automatic phasing of the generator to the network starts. The produced electrical energy is then supplied to the grid. The wiring diagram of the cogeneration unit is shown in fig. 1.

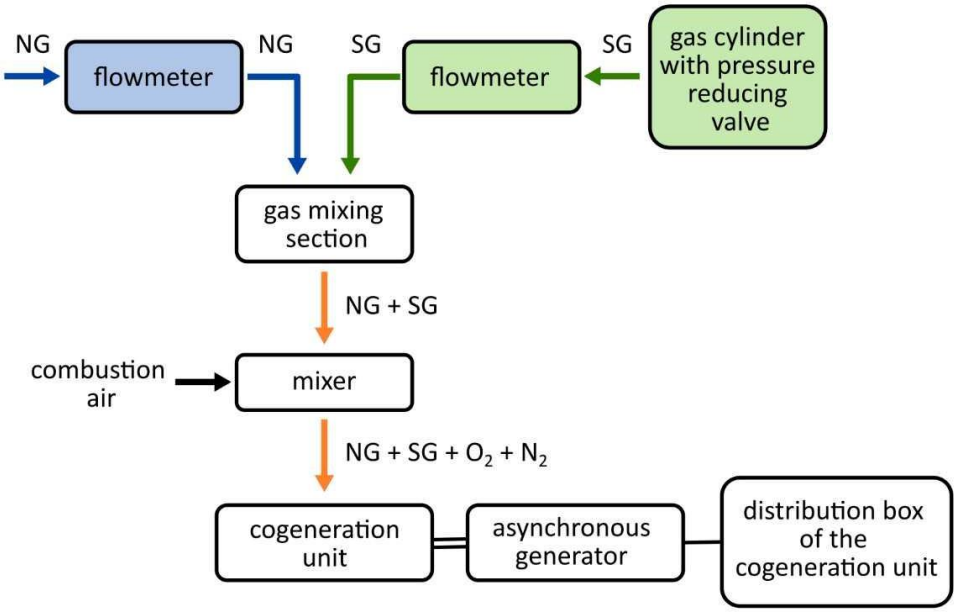

FIGURE 1: Wiring diagram of the measuring stand

Both natural gas and a mixture of natural gas (NG) and syngas (SG) were recovered in the cogeneration unit during the experiments. Mixing natural gas with syngas was carried out in the ratio shown in tab. 1.

TABLE 1
THE COMPOSITION OF THE FUEL MIXTURE

Fuel flow ($l \cdot min^{-1}$)			The composition of the fuel mixture (vol. %)			
natural gas	**synthesis gas**	**total flow rate**	**CH_4**	**H_2**	**CO**	**N_2**
86,0	0	86,0	100,0	0,0	0,0	0,0
81,2	4,8	86,0	94,70	2,51	2,23	0,56
76,8	9,2	86,0	89,84	4,81	4,28	1,07
68,5	17,5	86,0	80,67	9,16	8,14	2,03
60,9	25,1	86,0	72,27	13,13	11,67	2,92
52,5	33,5	86,0	62,99	17,53	15,58	3,90

In addition to the development of the change in the power of the electric generator depending on the composition of the fuel mixture (Fig. 2), the values of gaseous emissions arising from the co-combustion of NG and SG were also monitored (Table 2).

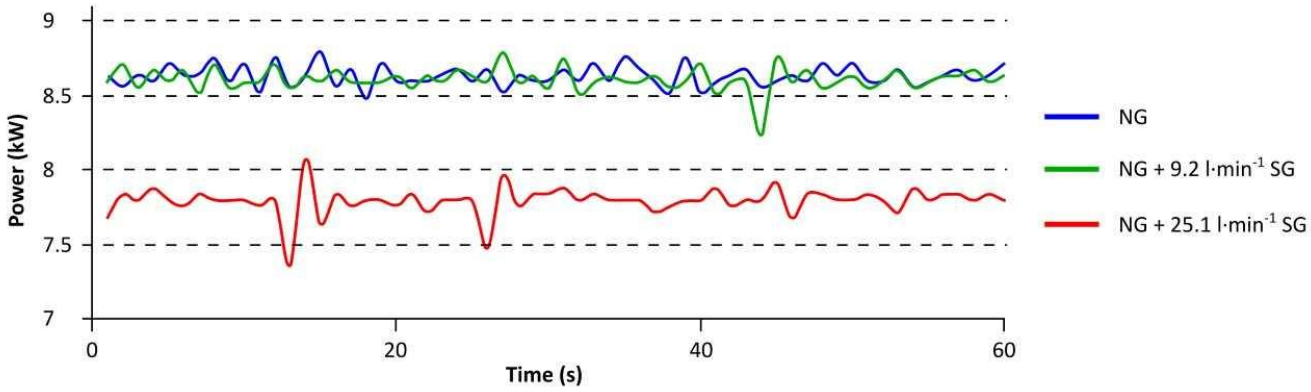

FIGURE 2: Power of the electric generator depending on the composition of the fuel mixture

The results from the flue gas analysis are shown v tab. 2.

TABLE 2
CONTENT OF O_2, CO, CO_2 IN FLUE GAS DETERMINED DURING THE EXPERIMENTS

Measured quantities for	Fuel					
	N+G	NG+SG	NG+SG	NG+SG	NG+SG	NG+SG
Flow of natural gas (l·min^{-1})	86	83.4	78	70	58.7	52
Flow of synthetic gas (l·min^{-1})	0	4.8	9.2	17.5	25.1	33.5
O_2 (%)	6.9	7	6.9	6.5	6.9	8.4
CO (ppm)	690.1	655.6	501	430	399	461
CO_2 (%)	6.74	6.91	6.87	7.11	6.92	6.18
T_S (°C)	198.4	201.8	201.5	207.8	205.9	203.4
T_V (°C)	16.2	16.5	16.7	17	17.2	17.5

III. DISCUSSION

An important property that plays an important role in determining the energy parameter of motor fuel is the calorific value, the value of which is defined by the concentration of combustible components and inert gas components contained in the fuel. Inert gases present in the fuel further affect the gas constant of the fuel, meaning on its density under the conditions of filling the cylinder engine with a fresh dose of fuel. The percentage of the individual gaseous components of the mixture also determines the resistance of the fuel against knocking, meaning transition of the normal course of combustion of the gas mixture in the cylinder to an uncontrolled state, characterized by self-ignition of the fuel before closing the top dead centre. The resistance of gaseous fuel against this unwanted phenomenon is expressed by the methane number, which can be determined by the sum of the methane numbers of the individual combustible components in the fuel reduced according to the volume share of the individual combustible components in the total content of combustibles in the fuel [7]. The presence of H_2 in the gas mixture causes a reduction in the knock resistance of the fuel, while inert gases such as CO_2 and N_2 increase the methane value. The high concentration of CO_2 and N_2 in the fuel also poses a risk for the quality of combustion [7].

During the measurement, the proportion of synthesis gas in the dosed mixture of gaseous fuel entering the cogeneration unit (tab. 2) increased, which resulted in a reduction of CO emissions in the flue gas. The increase in the CO emission value occurred at a synthesis gas flow rate of 33.5 l·min^{-1}. The given mixing ratio of gaseous fuels also caused an increase in the oxygen represented in the flue gas, with a simultaneous decrease in the share of CO_2. Taking these facts into account, it is possible to

state that the excess air for a specific gas mixture ratio is at a higher level compared to the optimal amount. However, the CO emissions arising in the volume of 461 ppm are still below the value of the CO emission limit in exhaust gas defined for gas engines. The development of CO emission production, depending on the synthesis gas flow, is shown in fig. 3.

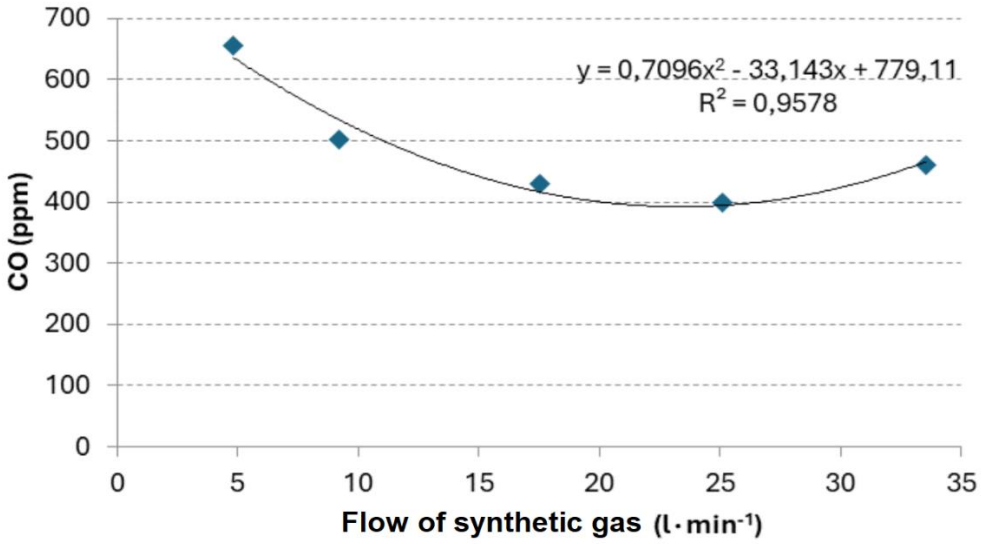

FIGURE 3: Development of CO emission production depending on synthesis gas flow

The CO emission limit in exhaust gases for stationary gas engines is set at 650 mg·Nm^{-3}. In the case of burning natural gas, as well as a mixture of natural gas and synthesis gas, on equipment directly intended for burning such fuel mixtures, together with the use of catalysts, it would be possible to suppress CO emissions to much lower values (compared to the results determined in the experiment). It is important, however, that the purified mixture of gaseous components forming the synthesis gas does not contain, or only contains a negligible amount of sulphur, fluorine and chlorine compounds. The increased value of carbon monoxide in the exhaust gases is caused by the incomplete combustion of the mixture of fuel and air in the cylinder of the experimental spark-ignition four-cylinder engine.

Other emissions in the flue gas are NOx emissions, whose emission limit for 1 Nm^3 of flue gas is 250 mg. This value is achievable in most cases for gas engines operating on natural gas. In the case of the production of a larger proportion of NOx emissions, the reduction can be achieved by a suitable change in the engine setting, which may consist in reducing the ignition advance or by depleting the fuel mixture. When burning a gaseous fuel mixture with a high content of inert gas, to achieve a high-quality course of the combustion process at n >> 1 (excess air), measures of a design nature consisting in the optimization of the combustion space and the ignition system in the engine cylinder are also required. The available type of flue gas analyser used did not allow the measurement of the amount of NOx in the flue gas (the basic equipment of the device does not have a probe for measuring NOx) produced in the experimental trial of energy recovery of synthesis gas using a cogeneration unit.

The aim of the energy recovery of the mixed synthesis gas mixture was also to monitor the change in the power parameters of the electric current generator depending on the change in the composition of the gaseous fuel (Fig. 2). By dosing the volume of 4.8 and 9.2 l of synthesis gas per minute into the flow of synthesis gas, it is possible to state that the changes in the power of the electric current generator are negligible. At the given flow rates, the volume of methane in the fuel mixture is above 89% and compared to the generator output when operating a cogeneration unit on natural gas, a decrease in the output of the electric power generator by 0.02 kW is recorded to a value of 8.62 kW. A more pronounced decrease in performance occurred when the synthesis gas flow rate was increased to 17.5 l·min^{-1}. In this phase of the measurement, the average value of the generator power was calculated at 8.2 kW. By increasing the proportion of synthesis gas in the fuel mixture, as was expected even before the experiment itself, the output of the cogeneration unit is further reduced. A leaner gas fuel mixture at a flow rate of 25.1 l·min^{-1} caused a drop in power to an average level of 7.8 kW. For a flow rate of 33.5 l·min^{-1}, the average power of the generator was calculated to be 7.2 kW. At the given output, the methane content in the fuel was approximately 63%. The efficiency of electricity production for the used fuel mixture was determined as the ratio of the energy content of the fuel to the electricity produced.

$$\eta_{\text{el}} = \frac{P_{\text{elG}}}{\frac{Q_{\text{pal}} \cdot Q_v}{t}} \cdot 100 \qquad (1)$$

Where:

Qpal is the calorific value of the fuel mixture ($J \cdot m^{-3}$),

Qv - volumetric flow of fuel ($m^3 \cdot s^{-1}$),

t - time of measurement (s),

PelG - average power of the electric power generator (W).

The dependence of the efficiency of electricity production on the synthesis gas flow is shown in fig. 4.

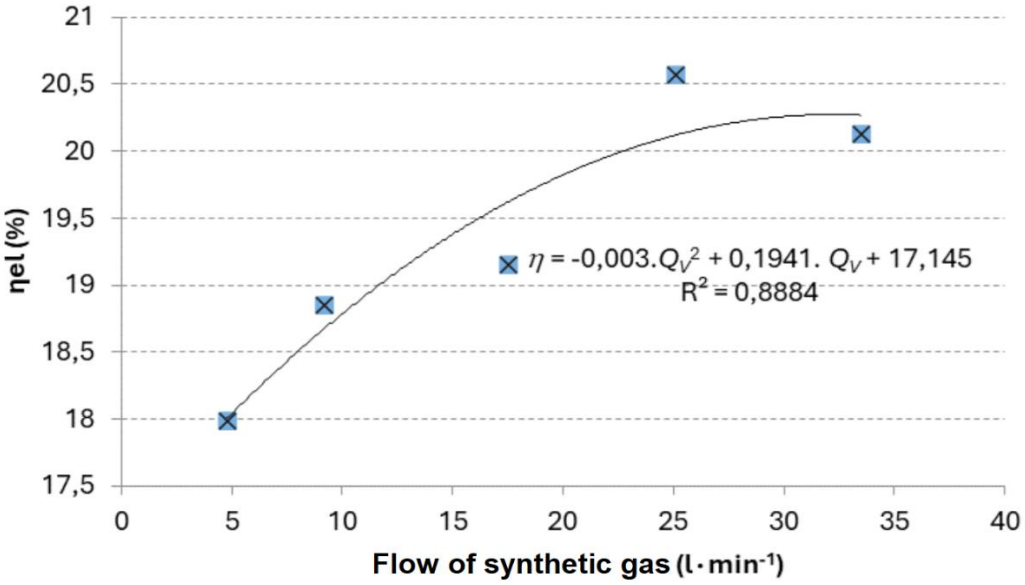

FIGURE 4: Dependence of the efficiency of electricity production on the synthesis gas flow

Based on the calculated values of the efficiency of electricity production, it can be concluded that the efficiency increases with the increasing proportion of synthesis gas in the gas fuel mixture. This tendency is visible until the moment of dosing of synthesis gas with a flow rate of 25.1 $l \cdot min^{-1}$. A further increase in SG flow will cause a breakdown and decrease in the efficiency of electricity production. This decrease is caused by the deterioration of the combustion process in the engine cylinder, which is also evidenced by the data measured using the flue gas analyser shown in tab. 2.

IV. CONCLUSION

In many cases, attention to the alternative energy market is devoted to solar energy, water and geothermal energy, while the energy stored in waste and their negative impact on the environment are often forgotten. The production of a gas mixture, with most of the hydrogen and carbon monoxide, represents a possible available source of energy and a high-quality input raw material for the chemical industry. Hydrogen, which forms a significant percentage of the gas mixture generated during high-temperature gasification, is also considered an alternative to replace fossil sources.

The significant deployment of hydrogen as a fuel requires a perfect mastery of technological and safety aspects and the creation of a sufficient portfolio of offered solutions, which will be based on modern hydrogen storage systems and alternative gaseous fuels with a high proportion of H2, as well as variable methods of hydrogen valorisation. One of the mentioned solutions enabling the transition of continuous transformation of technologies based on fossil fuels to green technologies is also the use and valorisation of secondary gaseous fuels. The conclusions valid for the implemented experimental trial can be defined in the following points.

Mixing the cleaned synthesis gas into the natural gas stream offers a real possibility of energy recovery of the synthesis gas produced in the gasification process. Gasification of waste with a high proportion of organic fraction, in addition to hygienic disposal and reduction of waste volume, also brings benefits in the form of energy recovery of otherwise unused waste, which usually ends up in managed or black landfills.

Dosing synthesis gas into the natural gas stream resulted in a reduction of CO emissions in the exhaust gases. By burning a mixture of synthesis gas and natural gas in cogeneration units, with fully automated control of the dosing of combustion air, fuel and the control of emerging emissions, it is possible to assume a more ecologically favourable operation of electricity production,

No operational problems were noted when burning the gaseous fuel mixture in accordance with tab.1. Reduced resistance to knocking in the engine cylinder was not noted at the volume fraction of hydrogen in the fuel at the level of 17.6 vol. %.

ACKNOWLEDGEMENTS

This paper was written with financial support from the VEGA granting agency within the project no. 1/0224/23 and from the APVV granting agency within the projects no. APVV-21-0274 and no. APVV-23-0266.

REFERENCES

[1] PUŠKÁR, M., BRESTOVIČ, T., JASMINSKÁ, N.: Numerical simulation and experimental analysis of acoustic wave influences on brake mean effective pressure in thrust-ejector inlet pipe of combustion engine. In: International Journal of Vehicle Design, 2015, Vol. 67, no. 1, p. 63-76., ISSN 0143-3369

[2] IWASAKI, H., SHIRAKURA, H., ITO, A.: A Study on Suppressing Abnormal Combustion and Improving the Output of Hydrogen Fueled Internal Combustion Engines for Commercial Vehicles. In: SAE Technical Paper Series, 2011. Available on: https://doi.org/10.4271/2011-01-0674.

[3] NATARAJAN, S., ABRAHAM, M., RAJESH, R., DAS, L.: DelHy 3W - Hydrogen Fuelled Hy-Alfa Three Wheeler, In: SAE Technical Paper Series. 2013. Available on: < https://doi:10.4271/2013-01-0224

[4] [4] MEHRA, R. K. et al.: Progress in hydrogen enriched compressed natural gas (HCNG) internal combustion engines - A comprehensive review, In: Renewable and Sustainable Energy Reviews, 2017, Volume 80, p. 1458-1498. Available on: https://doi.org/10.1016/j.rser.2017.05.061

[5] KOROLL, G. W. et al.: Burning velocities of hydrogen-air mixtures, In: Combustion and Flame, 1993, Volume 94, Issue 3, p. 330-340. Available on: < https://doi.org/10.1016/0010-2180(93)90078-H

[6] SCHROEDER, V., HOLTAPPELS, K.: Explosion Characteristics of Hydrogen-air and Hydrogen-Oxygen Mixtures at Elevated Pressures, In: International Conference on Hydrogen Safety, 2005, Available on: https://www.h2knowledgecentre.com/content/conference216#abstract_content

[7] BEROUN, S., ŠTECHR, V.: Výkonové a emisní parametry plynových motorů kogeneračních jednotek při provozu na paliva různékvality. [cit. 2014-03-20]. Dostupné na internete: www3.fs.cvut.cz/web/.../12241.../2006_100_01.pdf.

Analysis of the Selected Types of Waste Treatment by Plasma Technology: Part I

Lubomira Kmetova

Department of Energy Engineering, Technical University of Kosice, Slovakia

Received: 08 October 2024/ Revised: 15 October 2024/ Accepted: 21 October 2024/ Published: 31-10-2024

Abstract— *The series of articles (Analysis of the selected types of waste treatment by plasma technology. Part I., Part II.) discusses the processing of selected three types of waste using plasma technology. In this first part, the technology of plasma gasification and melting, is presented, as well as the processed types of waste. It involves the disposal of solid waste such as ash from municipal waste, silicone rubber and asbestos-cement material.*

Keywords— Thermal Treatment of Waste, Ash from Municipal Waste, Silicone Rubber and Asbestos-Cement Material, Plasma Technology.

I. INTRODUCTION

An undesirable consequence of human activity is the ever-increasing generation of waste. It is waste generated during the extraction of raw materials, then through the processing of primary raw materials, through treatment to the final product of human activity, which becomes waste after the end of its life cycle. At the beginning, it is necessary to point out once again that the raw material becomes waste, or another thing in the process of production and processing of emerging new products, a thing that has ended its life cycle but also a thing that is still functional, but its owner wants to get rid of it.

The production of the amount of waste depends on the economic activity of the state, as well as on the increase in the demands and activities of people. The oldest methods of waste disposal are thermal waste disposal processes after landfilling.

II. THERMAL PROCESSES OF WASTE TREATMENT

To use thermal disposal methods or waste processing were initially mainly driven by hygienic reasons, later there were also reasons for reducing the volume and weight of waste and thus saving the volume of landfills. Thermal methods are an integral part of the policy of a sustainable and integrated waste management system. [1]

Thermal waste disposal processes are characterized by high temperature and a greater rate of waste transformation compared to other biochemical and physio-chemical waste treatment processes. [2]

The following methods are distinguished:

2.1 Incineration:

Incineration is the most widespread method of disposal of municipal waste in the western countries of the EU. Incinerators are used for waste disposal with air access at operating temperatures of 850-1200 °C. They bring savings in the field of classic energy sources such as coal, natural gas and oil. Outputs from the combustion process are presented in Table 1. [2]

TABLE 1
OUTPUTS FROM THE COMBUSTION PROCESS

Produced gases	Polluting substances	Solid products
CO_2, water vapor	SO_2, NO_X, HCl, dioxins and furans (PCDD, PCDF), solid components in the form of chimney waste	Ash containing e.g. also ferrous and non-ferrous residues

2.2 Pyrolysis:

Pyrolysis is the heat treatment of waste materials in a pyrolysis furnace (at a temperature of 250 to 1650 ºC) without air access, or with limited air access and at reduced atmospheric pressure. The result of pyrolysis decomposition is liquid substances (pyrolysis oil) and gaseous substances (pyrolysis gas). These substances can be used as secondary raw materials (to produce benzene, toluene, etc.), or they are burned very efficiently (without significant production of emissions) in boilers to produce heat. [1]

Most heavy metals pass into solid pyrolysis residues and are not contained in emissions. Pyrolysis is a promising technology, especially for disposal of hazardous waste. So far, very few pyrolysis processes have been implemented for municipal waste compared to the number of implementations of waste incinerators. [1]

2.3 Gasification and Melting of Waste:

Unlike pyrolysis, an oxidizing agent is used in the gasification process of decomposition of the feed material.

In waste management, gasification and melting of waste using low-temperature plasma is mainly used. The basis of this technology is the creation of a plasma arc discharge from a stream of inert gas (Ar, N_2, etc.) or from gas enriched with oxygen. The plasma-forming gas is transformed into a plasma state with the help of a high-intensity electric field. High temperatures at the edges of the plasma arc discharge (1 200 – 1 800 °C) ensure a stable heat flow necessary for the thermal decomposition of waste.

Due to the high dissociation energy, the organic component of the waste is broken down into simple gas molecules. Inorganic waste components (in the form of liquid slag and metals) are periodically discharged through tap holes. The gas emerging from the plasma process can be used for energy purposes, depending on the presence of combustible components. Which partly eliminates the high energy demand of the technology. [3]

III. PLASMA AND WASTE MANAGEMENT

The technology of plasma gasification and melting is mainly used in metallurgical processes and in the synthesis of materials. In the developed countries of the world, it is also extended to the disposal of hazardous waste. Plasma treatment of waste takes place at temperatures above 1000 °C. It is a complex process that involves numerous physical and chemical interactions.

For the field of waste processing, it is necessary to highlight the advantages of this waste disposal technology [4]:

- High temperature of the plasma arc discharge, i.e. the possibility of thermal treatment of waste at a temperature of several °C,
- High rate of particle heating in connection with the heat exchange between the particle and the plasma,
- The high rate of heating is therefore also associated with the rapid decomposition of part of the waste of organic origin with the explosive release of volatile substances,
- UV radiation, which is emitted from a weakly ionized plasma, ensures the decomposition of halogenated hydrocarbons,
- Plasma technology products are predictable and environmentally acceptable if technological procedures are followed,
- Wide spectrum use.

Laboratory equipment for plasma gasification and melting is used at Faculty of Mechanical Engineering, Technical University of Košice, Department of Energy Engineering, where experiments were carried out with various types of waste commodities. A 10 kVA reactor generates a plasma arc discharge between:

1) Cathode – a hollow graphite electrode through which the plasma-forming gas (N_2) is supplied and
2) Anode – a graphite crucible that is placed at the bottom of the plasma reactor.

The plasma reactor also contains a reservoir and a screw-dosing device for the charged commodity, as well as a cyclone separator and a device for cleaning the generated synthesis gas.

The plasma reactor contains a heat-resistant alumina lining, an electrode sliding mechanism, a graphite crucible and accessories providing power supply.

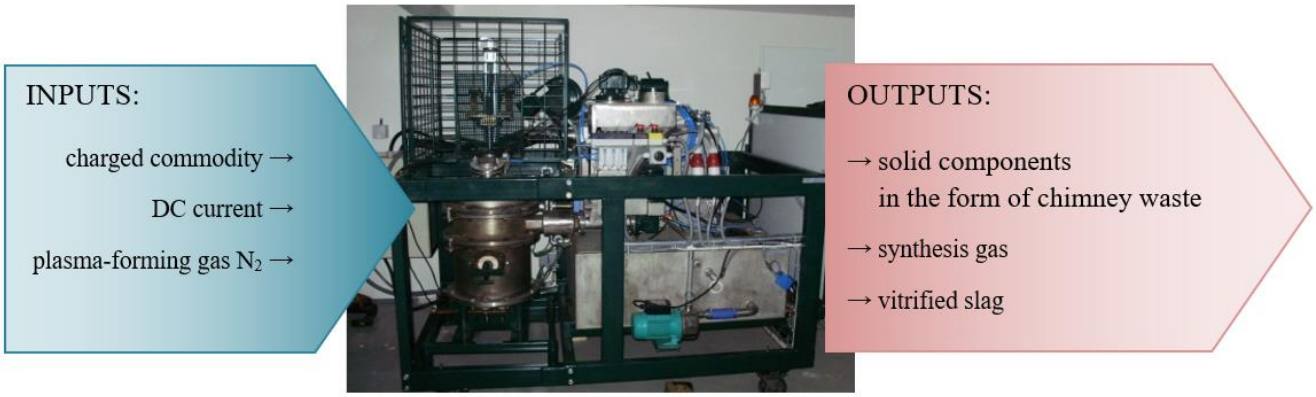

FIGURE 1: Laboratory plasma reactor with its inputs and outputs

There are technological openings on the reactor lid and shell, which are used for:

- Service purposes,
- Input of hollow graphite electrode,
- Input of waste commodity,
- Extraction of synthesis gas,
- Removal (tapping) of slag and alloy.

The generated plasma arc discharge heats and melts the charged commodity in a dependent connection. The melt is concentrated at the bottom of the reactor in two separate phases, slag and metal alloy, which are subsequently tapped from the reactor through tapping holes.

Together with slag and metal alloy (if the input commodity also contains metal parts), gaseous products are also produced - a mixture of gaseous components containing solid pollutants, which are removed in a cyclone separator.

Cooling of the electrode is provided by water-cooling as well as by the supply of the plasma-forming gas itself, i.e. of nitrogen, which also prevents syngas leakage at the point of entry of the electrode into the reaction chamber of the reactor. The introduction of nitrogen also prevents oxidation of the graphite electrode.

Monitoring of several basic parameters is important for the proper course of the waste treatment process by plasma gasification and melting:

- Operating temperature,
- Current and voltage parameters,
- Total power input of the technological line,
- Cooling medium flow,
- Mode and rate of dosing of the commodity being charged.

IV. WASTE PROCESSED BY PLASMA TECHNOLOGY

Three waste commodities were subjected to plasma gasification and melting at our workplace:

1. Fly ash from solid municipal waste,
2. Waste containing asbestos,
3. Silicone rubber.

4.1 Fly ash from solid municipal waste:

During the incineration of municipal waste, solid and gaseous products are formed:

- Gaseous emissions,

- Ash (cinder)
- and Fly ash.

Electrostatic or mechanical separators within the flue gas cleaning system capture fly ash, as a by-product of heating and energy production. The mineralogical, granulometric and chemical composition of the ash depends on the type of incinerated batch, the type of focus or the technical method of solving the incineration process. Its use as a secondary raw material is therefore subject to certain requirements arising from the standards.

FIGURE 2: Fly ash from municipal solid waste

Cinder and fly ash from municipal waste make up 25 to 30 % of the weight, but only 10 to 15 % of the original waste volume. Toxic substances are concentrated in fly ash and cinder, so although the area required for their storage is significantly reduced, such waste must be stored in controlled landfills, it is necessary to ensure their stabilization. For example, it involves its fixation with cement, extraction with acids or stabilization with chemical additives. Ultimately, the goal of the stabilization processes is to solidify this fine dust fraction of waste.

In the most widespread method of ash solidification, i.e. fixation of fly ash in a silicate matrix using the cementation method reduces the leaching of toxic fly ash substances but does not solve the problem of placing fly ash in a landfill.

On the contrary, a more suitable technology for disposing of fly ash is its melting in a thermal-chemical process, the so-called vitrification. The resulting product is an extremely stable glass matrix.

4.2 Waste containing asbestos:

Asbestos is the technical name of a group of minerals that can be divided into flexible and brittle fibers. It is a fibrous silicate that occurs in several forms (Figure 3).

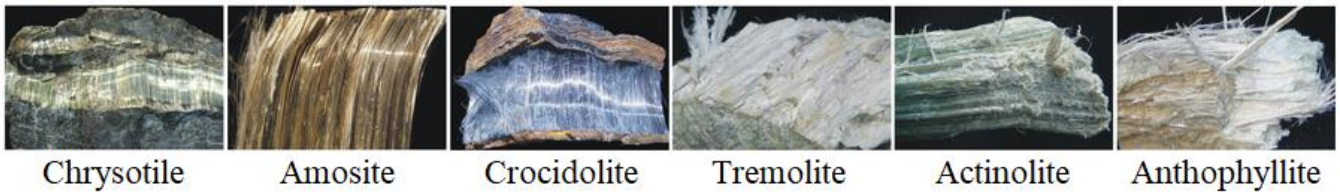

FIGURE 3: Forms of asbestos [5]

In the last century, due to its properties, asbestos was used in many branches of industry. Asbestos stands out for the following properties:

- Excellent resistance to temperatures and chemicals,
- High tensile strength,
- Flexibility,
- High stability under normal conditions.

However, its high danger lies in the release of fibres of microscopic dimensions into the air during the natural weathering of building materials, as well as during unprofessional handling or processing (cutting, abrasion or vibration).

The harmful effects of asbestos fibres on the human body have been proven. Due to their hardness, microscopic asbestos fibres with dimensions of approximately 5 micrometres and a thickness of 3 micrometres easily penetrate the lungs when inhaled. Long-term exposure to asbestos fibres on the body can cause diseases such as asbestosis or lung cancer.

However, there are several studies dealing with asbestos inerting technologies, e.g.:

- High temperature processing (firing, melting, vitrification) [6, 7],
- Microwave heating [8 – 10],
- Hydrothermal transformation [11, 12],
- Non-thermal technologies [13, 14].

4.3 Silicone rubber:

Rubber is a material of natural or synthetic origin that belongs to the category of polymer materials. It is a material with a high degree of elasticity. It is the basic building block for rubber production.

FIGURE 4: Products of silicone rubber [15]

The rubber production process takes place using various technologies for processing rubber compounds, which are divided into [16]:

- Preparatory (mixing and kneading),
- Basic (extrusion and rolling),
- Associated (pressing, extrusion and injection moulding),
- Supplementary (joining and surface treatments).

The necessary operations for processing rubber compounds into the final product are:

1) Mixing rubber compounds:

Rubber products are composed of several components that must be mixed homogeneously. Fillers, antidegradants, plasticizers, and vulcanizing agents are practically always used in the formulation of rubber compounds. Depending on the type of specific product, pigments, blowing agents, adhesion agents, peptizing agents, or reinforcing materials can also be part of rubber systems. In addition to plasticizers, which are not defined as solvents, no organic solvents are used in this stage of the preparation of rubber compounds.

2) Processing of rubber compounds:

Rolling (calendering) and extrusion technologies are mainly used to shape rubber compounds. The rolling technology is used to produce the rubber bands themselves, which are used in the assembly of finished products (e.g. tire casings, conveyor belts), for impregnation and rubberization of textiles, friction application and others. Extrusion technology is used for the preparation of semi-finished products of more complex products (e.g. tire production), or to produce final products (e.g. hoses, gaskets, various profiles), if the extruded profile is simultaneously pulled through the zone where it is vulcanized (continuous vulcanization). No organic solvents are used in this stage of preparation of rubber compounds.

3) Vulcanization:

Vulcanization is the process of transforming a plastic rubber mixture into a highly elastic final product - vulcanizate, or what is commonly referred to as rubber. It acquires highly elastic properties as a result of the creation of physical and especially chemical cross-links between segments of rubber chains, during reactions of functional groups of rubbers with functional groups of vulcanizing agents (Figure 5).

This creates a spatial three-dimensional network of the rubber matrix, in which the other components of the rubber mixtures are dispersed, dissolved, physically, or chemically bound to rubber chains. The vulcanization process usually takes place at elevated temperature (150-200 °C) and pressure. Pressing, extrusion and injection technologies are used for the vulcanization of rubber compounds. No organic solvents are used in this stage of preparation of rubber compounds.

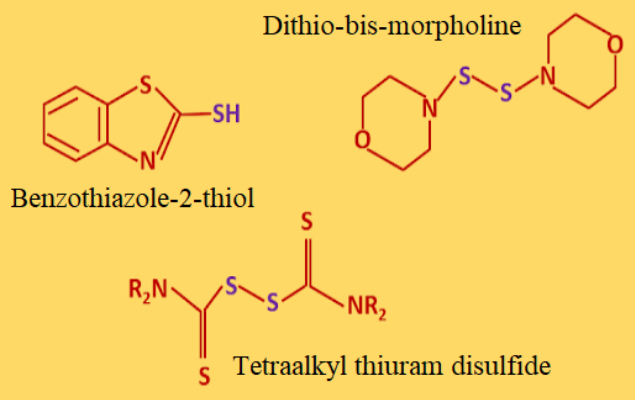

FIGURE 5: Vulcanization initiators [17]

Silicone rubber recycling is quite complicated, unlike plastic, paper or glass recycling which is straightforward. When silicone rubber is recycled, it is possible to reduce the amount of this waste and thereby reduce primary production costs. There are two main ways to recycle silicone rubber: moulding and extrusion.

During pressing, the silicone rubber is melted and formed into a new shape. This method is often used to recycle waste from production or to recycle used products.

In extrusion, the silicone rubber is melted and pushed through a die to form new pellets or "noodles". These pellets can be used to make new products or sold as is.

When silicone rubber is reprocessed, its properties are gradually degraded.

V. CONCLUSION

It is very important to focus more strongly on appropriate methods of waste processing, as its generation has a constantly growing trend. Thermal methods of waste disposal represent reliable and effective methods of disposing of various forms of waste. After classic waste incineration, plasma gasification and waste melting devices are used. Several studies have already been carried out to assess the suitability and effectiveness of using the plasma thermal process. To verify the suitability of plasma waste processing technology, 3 different types of waste were selected – fly ash from municipal solid waste, waste containing asbestos and silicone rubber.

ACKNOWLEDGEMENTS

This paper was written with financial support from the granting agency VEGA within the Project Solution No. 1/0532/22.

REFERENCES

[1] VANTÚCH, M. Termická likvidácia odpadu - racionálny spôsob zhodnocovania komunálneho odpadu. Odborný seminár: 11.09.2014 Ostrava. [cit. 15.10.2024]. Available at: https://ceet.vsb.cz/export/sites/ceet/vec/.content/galerie-souboru/240-vantuch.pdf

[2] ČARNOGURSKÁ, M., LÁZÁR, M. Plazmové spracovanie a zhodnocovanie odpadu. Strojnícka fakulta TUKE 2013. 1.vydanie. 164 s., ISBN 978-80-553-1514-0.

[3] IMRIŠ, I., KLENOVČANOVÁ, A. Splynovanie odpadov v plazmovej peci. 2001. [cit. 15.10.2024]. Available at: https://www.tzb-info.cz/600-splynovanie-odpadov-v-plazmovej-peci

[4] LÁZÁR, M., ČARNOGURSKÁ, M. AND BRESTOVIČ, T. Vysokoteplotné technológie spracovania odpadu. Azbest a popolček. Strojnícka fakulta TUKE, 2018. 1.vydanie. 201 s., ISBN 978-80-553-2756-3.

[5] COLBY COLLEGE. Asbestos Awareness. [cit. 15.10.2024]. Available at: https://www.colby.edu/humanresources/wp-content/uploads/sites/170/2015/05/Asbestos-Awarness-Safety-Talk.pdf

[6] GUALTIERI, A.F.; TARTAGLIA, A. Thermal decomposition of asbestos and recycling in traditional ceramics. In: Journal of the European Ceramic Society, 2000, Vol. 20, Issue 9, p. 1409-1418. ISSN 0955-2219.

[7] ZAREMBA, T.; PESZKO, M. Investigation of the thermal modification of asbestos wastes for potential use in ceramic formulation. In: Journal of Thermal Analysis and Calorimetry, 2008, Vol. 92, Issue 3. p. 873-877. ISSN 1388-6150.

[8] DI VESTO, P.L.; ANNIBALI, M.; CARDELLINI, F.; MARUCCI, G.; SICA, M.; PORTOFINO, S. Asbestos inertization through microwave thermal treatment: materials characterization and economic evaluation. In: Materials Research Innovations, 2004, Vol. 8, no. 1. p. 58-62. ISSN 1432-8917.

[9] LEONELLI, C.; VERONESI, P.; BOCCACCINI, D.N.; RIVASI, M.R.; BARBIERI, L.; ANDREOLA, F.; LANCELLOTTI, I.; RABITTI, D.; PELLACANI G.C. Microwave thermal inertisation of asbestos containing wastes and its recycling in traditional ceramics. In: Journal of Hazardous Materials, 2006, Vol. 135, Issue 1-3, p. 149-155. ISSN 0304-3894.

[10] AVERROES, A.; SEKIGUCHI, H.; SAKAMOTO, K. Treatment of airborne asbestos and asbestos-like microfiber particles using atmospheric microwave air plasma. In: Journal of Hazardous Materials, 2011, Vol. 195. p. 405-413. ISSN 0304-3894.

[11] ANASTASIADOU, K.; AXIOTIS, D.; GIDARAKOS, E. Hydrothermal conversion of chrysotile asbestos using near supercritical conditions. In: Journal of Hazardous Materials, 2010, Vol. 179, Issue 1-3. p. 926-932. ISSN 0304-3894.

[12] KOZAWA, T.; ONDA, A.; YANAGISAWA, K.; CHIBA, O.; ISHIWATA, H.; TAKANAMI, T. Thermal decomposition of chrysotile-containing wastes in a water vapor atmosphere. In: Journal of the Ceramic Society of Japan, 2010, Volume 118, Issue 1384, p. 1199-1201. ISSN 1882-0743.

[13] PLESCIA, P.; GIZZI, D.; BENEDETTI, S.; CAMILUCCI, L.; FANIZZA, C.; DE SIMONE, P.; PAGLIETTI, F. Mechanochemical treatment to recycling asbestos-containing waste. In: Waste Management, 2003, Volume 23, Issue 3, p. 209-218. ISSN 0956-053X.

[14] YANAGISAWA, K.; KOZAWA, T.; ONDA, A.; KANAZAWA, M.; SHINOHARA, J.; TAKANAMI, T.; SHIRAISHI, M. A novel decomposition technique of friable asbestos by CHClF2-decomposed acidic gas. In: Journal of Hazardous Materials, 2009, Volume 163, Issue 2-3, p. 593-599. ISSN 0304-3894.

[15] Cheng, A. An overview of the silicone recycling process. Rubber World, vol. 264, no. 3. June 2021. p. 32-34.

[16] Baran, P. et al. Štúdia o referenčných technikách zodpovedajúcich BAT pre zariadenia používajúce organické rozpúšťadlá. November 2018. p. 247-248. [cit. 15.10.2024]. Available at: https://www.enviroportal.sk/dokument/f/studia-o-referencnych-technikach-zodpovedajucich-bat-pre-zariadenia-pouzivajuce-organicke-rozpustadla-ktore-nespadaju-p.pdf

[17] Vulcanization Initiators. October 2020. [cit. 15.10.2024]. Available at: https://www.elementalchemistry.in/2020/10/vulcanization-of-rubber.html

[18] ECO USA. [cit. 15.10.2024]. Available at: https://www.ecousarecycling.com/silicone-rubber-recycling-process/.

AD Publications
Sector-3, MP Nagar, Bikaner,
Rajasthan, India
www.adpublications.org, info@adpublications.org